NASA CR-54591
GE R69AEG103

# EXPERIMENTAL EVALUATION OF OUTER CASE BLOWING OR BLEEDING OF SINGLE STAGE AXIAL FLOW COMPRESSOR

## PART V - PERFORMANCE OF PLAIN CASING INSERT CONFIGURATION WITH DISTORTED INLET FLOW



by

C.C. KOCH



prepared for

**NATIONAL AERONAUTICS AND SPACE ADMINISTRATION**

CONTRACT NAS 3-7618

AIRCRAFT ENGINE TECHNICAL DIVISION
AIRCRAFT ENGINE GROUP
GENERAL ELECTRIC
LYNN, MASSACHUSETTS/CINCINNATI, OHIO

Requests for copies of this report should be referred to

National Aeronautics and Space Administration
Office of Scientific and Technical Information
Attention: AFSS-A
Washington, D.C. 20546

# EXPERIMENTAL EVALUATION OF OUTER CASE BLOWING OR BLEEDING OF SINGLE STAGE AXIAL FLOW COMPRESSOR
## PART V - PERFORMANCE OF PLAIN CASING INSERT CONFIGURATION WITH DISTORTED INLET FLOW


BY

C. C. KOCH


prepared for

NATIONAL AERONAUTICS AND SPACE ADMINISTRATION


MAY, 1969

CONTRACT NO, NAS3-7618

Technical Management
NASA Lewis Research Center
Cleveland, Ohio

Everett Bailey, Project Manager



AIRCRAFT ENGINE TECHNICAL DIVISION
AIRCRAFT ENGINE GROUP
GENERAL ELECTRIC

LYNN, MASSACHUSETTS/CINCINNATI, OHIO

EXPERIMENTAL EVALUATION OF OUTER CASE BLOWING OR BLEEDING OF SINGLE STAGE AXIAL FLOW COMPRESSOR

PART V - PERFORMANCE OF PLAIN CASING INSERT CONFIGURATION WITH UNDISTORTED INLET FLOW AND BOUNDARY LAYER TRIP

BY

C. C. Koch and L. H. Smith, Jr.

## ABSTRACT

An isolated transonic rotor having an aspect ratio of 4.5 was tested under several conditions of distorted inlet flow. Overall and stalling performance was determined for each inlet condition, and extensive surveys of flow conditions were made for one case of circumferential inlet distortions. Although this rotor stalls at the pitchline with undistorted inlet flow, the tip of the rotor is limiting when inlet flow distortions exist.

The effect of intense circumferential inlet distortions was to reduce stalling weight flow by such a large extent that stall margin increased despite a reduction in stalling total-pressure ratio. The same effect was observed with less intense circumferential inlet distortions at the lower speeds, but at design speed there was less of a reduction in flow and a slight loss in stall margin. One radial inlet distortion condition was tested, and produced a substantial loss in stall margin.

## SUMMARY

The overall objective of this program is to investigate outer casing boundary layer control as a means of increasing the weight flow range of an isolated transonic rotor. The rotor used in the investigation has an aspect ratio of 4.5, an inlet hub-tip radius ratio of 0.5, a design tip diffusion factor of 0.45 and operates at a design tip speed of 1120 feet per second. This report documents the performance of the rotor when subjected to inlet flow distortions in its baseline configuration without casing boundary layer control devices.

Overall and stalling performance were measured for one tip radial and four circumferential inlet distortion conditions. Rotating stall originated at the tip of the rotor when operated with inlet distortions although this rotor stalls at the pitchline with undistorted inlet flow. Radial inlet distortion produced a large loss in stall margin relative to the undistorted inlet stall line, but the stall margin increased with intense circumferential inlet flow distortions. The effect of intense circumferential inlet distortions was to reduce stalling weight flow by such a large amount that stall margin increased despite a reduction in stalling total-pressure ratio. The same effect was produced by less intense circumferential inlet distortions at the lower speeds, but at design

speed there was less of a reduction in stalling weight flow and a slight loss in stall margin.

Extensive circumferential surveys of flow conditions were made during testing with one of the intense circumferential inlet distortions by rotating the inlet distortion screen relative to the instrumentation. These surveys showed that a region of separated flow existed in the rotor behind the distortion screen. The interaction of this separated zone with the flow in the rest of the annulus is believed to cause the increased stall margin.

## INTRODUCTION

It is recognized that the use of high-aspect-ratio blading in aircraft gas turbine engines offers the potential of designing lighter, more compact units. The performance of such stages has not always been satisfactory, however, in that they generally have been found to have less weight flow range than similar stages with lower aspect-ratio blading (references 1 and 2). Reduced weight flow range typically results in reduced stall margin, especially in cases where the compressor must operate with inlet flow distortions.

The objective of this program is to investigate outer case blowing and bleeding in order to determine their effectiveness in increasing the weight flow range of an isolated high-aspect-ratio rotor under conditions of distorted as well as undistorted inlet flow. The designs of the rotor and of the blowing and bleeding configurations are presented in reference 3. The undistorted inlet performance of the rotor with the plain casing installed (without casing boundary layer control) is documented in reference 4. The performance of the rotor when tested with outer case blowing and bleeding is presented in references 5 and 6 respectively, for distorted and undistorted inlet flow.

This report presents the performance of the rotor with the plain casing insert configuration when tested with one radial and four circumferential inlet flow distortions. The overall performance and the effect of distortion on stall margin were determined for each inlet condition. In addition, detailed surveys of inlet and discharge conditions were made for the case of a severe circumferential distortion which covered 90° of the inlet annulus. These were obtained by rotating the screen to various positions relative to the fixed rakes and traverse probes.

## SYMBOLS

The following symbols are used in this report:

| | |
|---|---|
| $A$ | flow area, in$^2$ |
| $A_j$ | area represented by each discharge rake element. This is the area of an annulus bounded either by radii midway between those of the two adjacent elements or by the hub or casing, in$^2$ |
| $C_h$ | enthalpy-equivalent static-pressure-rise coefficient, |

$$C_h = \frac{2gJc_p t_1\left[\left(\frac{P_2}{P_1}\right)^{\frac{\gamma-1}{\gamma}} - 1\right] - (U_2^2 - U_1^2)}{V_1'^2}$$

| | |
|---|---|
| $C_p$ | static - pressure-rise coefficient, |

$$C_p = \frac{p_2 - p_1}{P_1' - p_1}$$

| | |
|---|---|
| $c_p$ | specific heat at constant pressure, Btu/lb-°R |
| $D$ | diffusion factor |

$$D = 1 - \frac{V_2'}{V_1'} + \frac{r_2 V_{\theta 2} - r_1 V_{\theta 1}}{2\bar{r}\,\sigma\, V_1'}$$

| | |
|---|---|
| $g$ | acceleration due to gravity, 32.174 ft/sec$^2$ |
| $i$ | incidence angle, difference between air angle and camber line angle at leading edge in cascade projection, deg |
| $J$ | mechanical equivalent of heat, 778.161 ft-lb/Btu |
| $M$ | Mach number |
| $P$ | total or stagnation pressure, psia |
| $P_j$ | arithmetic average total pressure at j immersion, psia |
| $p$ | static or stream pressure, psia |

| | |
|---|---|
| $r$ | radius, in |
| $\bar{r}$ | mean radius, average of streamline leading-edge and trailing-edge radii, in |
| $T$ | total or stagnation temperature, °R |
| $T_j$ | arithmetic average total temperature at j immersion, °R |
| $t$ | static or stream temperature, °R |
| $U$ | rotor speed, ft/sec |
| $V$ | air velocity, ft/sec |
| $V_{zj}$ | average axial velocity at j immersion, ft/sec |
| $W$ | weight flow, lb/sec |
| $z$ | displacement along compressor axis, in |
| $\beta$ | air angle, angle whose tangent is the ratio of tangential to axial velocity, deg |
| $\gamma$ | ratio of specific heats |
| $\delta$ | ratio: $\frac{\text{total pressure}}{\text{standard pressure}}$, $\frac{\text{psia}}{14.696\ \text{psia}}$ |
| $\delta^{\circ}$ | deviation angle, difference between air angle and camber line angle at trailing edge in cascade projection, deg |
| $\varepsilon^{\circ}$ | meridional angle, angle between tangent to streamline projected on meridional plane and axial direction, deg |
| $\theta$ | ratio: $\frac{\text{total temperature}}{\text{standard temperature}}$, $\frac{°\text{R}}{518.688°\text{R}}$ |
| $\theta^{\circ}$ | angular displacement about compressor axis, deg |
| $\eta$ | efficiency |
| $\kappa^{\circ}$ | angle between cylindrical projection of the blade camber line at the leading or trailing edge and the axial direction, deg |
| $\rho$ | static or stream density, lb-sec$^2$/ft$^4$ |
| $\sigma$ | solidity, ratio of chord to spacing |
| $\psi$ | stream function; $\psi_h = 0$, $\psi_c = 1$ |
| $\bar{\omega}$ | total-pressure-loss coefficient |

Subscripts:

| | |
|---|---|
| ad | adiabatic |
| an | annulus value |
| avg | arithmetic average at any plane |
| c | casing at any plane |
| d | downstream |
| h | hub at any plane |
| in | inlet |
| j | immersion number |
| m | meridional direction |
| p | polytropic |
| s | suction surface |
| u | upstream |
| z | with respect to axial displacement |
| $\theta$ | with respect to circumferential displacement |
| 1 | leading edge |
| 2 | trailing edge |
| 0.05, 0.65, 0.90, 1.54, 1.90, 3.50 | instrumentation plane designations (figures 1 and 2) |

Superscripts:

| | |
|---|---|
| * | critical flow condition |
| ' | relative to rotor |

## APPARATUS AND PROCEDURE

### Test Rotor Design

A high-aspect-ratio transonic rotor was designed as an instrument for evaluating the effects on performance and operating range of outer casing blow and bleed configurations on stages of this type. The overall characteristics of the rotor design are contained in the following list.

1. Rotor tip speed, 1120 ft/sec.
2. Inlet hub-tip radius ratio, 0.50.
3. Total-pressure ratio, 1.47, radially constant.
4. Corrected weight flow per unit annulus area, 39.32 lb/sec-sq ft.
5. Rotor tip solidity, 1.0.
6. Rotor tip relative Mach number 1.2.
7. Rotor tip diffusion factor, 0.45.
8. Rotor blade aspect ratio 4.5.
9. Rotor blade section; double-circular-arc on cylindrical sections.
10. Rotor chord, 1.772 in., radially constant.
11. Rotor maximum thickness-chord ratio, 0.085 at hub, 0.03 at tip.
12. Number of rotor blades, 60.
13. Rotor tip diameter, 34 in.
14. Corrected weight flow, 187 lbs/sec.

The rotor tip diffusion factor of 0.45 is somewhat higher than is common practice for stages with a radius ratio of 0.5. The moderately large tip loading was selected with the expectation that the boundary layer control devices to be investigated would permit operation at loading levels that exceed those given by conventional design criteria. The remaining items were selected as being typical of a compressor front stage, the stage most likely to require application of a boundary layer control device. Full details of the methods employed in the design of this rotor and the resulting design parameters are presented in reference 3.

### Test Facility

Performance tests of this rotor were made in General Electric's House Compressor Test Facility, at Lynn, Massachusetts. The general aspects of the test set-up are shown in figure 4 of reference 4. The test rotor draws air from the atmosphere through two banks of filters. The first filter bank is intended to remove 22% of the particles larger than 3-5 microns (dust spot test). The second filter tank is intended to remove 90-95% of the remaining particles down to the same size. The air then passes through a coarse wire inlet screen and into the bellmouth. Downstream of the test rotor, outlet guide vanes are used to remove most of the swirl. In the exit assembly the air is split into two streams. The inner air stream is passed into an exit pipe containing a flow straightener and a venturi flow meter and then is exhausted to the atmosphere. The outer air stream passes through a slide cylindrical throttle valve and into a collector, then into two pipes, each of which contains a flow straightener and a venturi flow meter, and is finally discharged to the atmosphere.

Power to drive the test rotor is provided by a high-pressure non-condensing steam turbine rated at 15,000 horsepower.

## Instrumentation

Schematic views of the instrumentation provided for the testing are shown in figures 1 and 2, and photos of the rakes themselves are shown in figure 3. Inlet total temperature was measured by twenty-four (24) thermocouples distributed on the inlet screen. During all tests four 5-element inlet distortion total-pressure rakes located at plane 0.65 were used to obtain the inlet total pressure. Immersions of the 5 elements on each rake corresponded to the design streamlines which passed through the 10%, 30%, 50%, 70% and 90% immersions at plane 1.54. A 1?-element boundary layer rake was immersed from the outer casing at plane 0.65 ahead of the rotor.

Hot wire anemometer data were taken with three shielded probes located behind the rotor at plane 1.54. These were used to obtain traces on high-speed paper tape from which the number, rotative speed, and radial extent of the rotating stall cells could be determined.

Outlet total pressures and temperatures were measured at plane 1.9 by 4 fixed rakes of each type. Immersions of the 5 elements on each rake again corresponded to the design streamlines at the 10%, 30%, 50%, 70% and 90% annulus height positions at plane 1.54. The discharge rakes at plane 1.9 were ahead of the outlet guide vanes in a region of swirling flow. These rakes were therefore rotated 37.5° from the axial direction to match the pitchline swirl angle of the flow at the design condition. Kiel type sensors were used to obtain accurate data over a wide range of flow angles.

Numerous static pressure taps were located on the hub and casing throughout the flowpath. At measuring planes where fixed rakes or traverse probes were located, static pressures at the hub and casing were measured at more than one circumferential position (figure 2).

During the circumferential distortion test with the heavy 90° screen, angle-seeking cobra probes were installed at plane 0.90 and 1.54 in order to obtain radial and circumferential surveys of inlet and discharge flow angle. Two probes were located at 25° and 298° from top center at plane 0.90, and two were placed at 16° and 295° at plane 1.54. During the test these were immersed to correspond to the design streamlines which passed through the 10%, 50% and 90% immersions at plane 1.54.

## Distortion Screens

Five inlet airflow distortion patterns were tested with the plain casing insert configuration; all were produced by mounting distortion screens at plane 0.10 approximately 26% of a rotor diameter ahead of the rotor's leading edge. The distortion screens were mounted on a support screen which covered the entire inlet annulus and which was made of 0.092 inch diameter wire at 3/4 inch spacing. Photographs of the distortion screens are shown in figure 4.

The least porous, or heavy, distortion screens had 54% blocked area and were made of 20 mesh 0.016 inch wire diameter material. These were designed to produce a pattern at plane 0.65, the inlet measuring station, having a value of $(P_{max}-P_{min})/P_{max} = 0.20$ at the design weight flow of 187 lbs/sec. The more porous, or light, distortion screens had 35% blocked area and were made of 10 mesh 0.020 inch wire diameter material. These were designed to produce a value of $(P_{max}-P_{min})/P_{max} = 0.10$ at a flow of 187 lbs/sec.

The single radial distortion screen was made of the heavy screen material and covered the outer 40% of the inlet annulus, figure 4 (a). One circumferential distortion screen was also made of this heavy material; this screen covered a 90° sector of the inlet annulus from hub to tip, figure 4 (b). Two circumferential screens were made of the light material; one covered a 90° sector, figure 4 (c), and the other covered 180°, figure 4(d). The final circumferential distortion screen, the 120° rounded pattern, used both types of material. The center 60° sector was made of the heavy screen, while a 30° sector at each side of the center panel was made of the light screen, figure 4 (e).

Originally it had not been planned to rotate the distortion screens, so no automatic screen positioning equipment was provided. Normally the support screen was clamped in place by the casing flange at plane 0.10. In order to change screen position, the casing was shimmed apart so that the support screen could be moved. A small slot was machined in the support screen outer ring every 10° around the circumference, and an opening big enough for a screwdriver blade was cut in the casing flange. The screen could then be rotated manually by ten degree increments, and was locked in place by a set screw inserted into one of the slots in the support screen outer ring.

## Test Procedure

A separate test run was conducted to obtain overall and stall performance of the rotor with each of the five inlet flow distortions. The first part of each test run was devoted to determining the stall points at 70%, 90% and 100% of design rotor speed. Overall performance data from the fixed instrumentation were then obtained at each of these speeds at various discharge throttle valve settings between maximum flow and the limit of stall-free operation. Finally whenever blade stresses permitted, overall performance was recorded at each speed while in stall and at the point where the stalls cleared.

An additional test was conducted with the heavy 90° circumferential distortion screen installed, during which the screen was rotated to approximately fifteen angular positions. Overall performance data and flow angle traverses were obtained for each screen position. These data gave a much more complete indication of the radial and circumferential variations of fluid conditions than could be obtained from the usual overall performance tests.

Testing in the Unstalled Region. Throttle settings at which data were recorded in the unstalled region of operation were selected to give an approximately even spacing of the point on the compressor performance map speed lines. For overall performance data points, the inlet total pressure was determined by taking the arithmetic average of all elements on the four inlet total-pressure distortion rakes located at plane 0.65. The discharge total-pressure and total-temperature ratios were obtained by the mass-weighting procedure explained in reference 4. Although the above methods of obtaining inlet and discharge conditions cannot really be justified for the case of a circumferential inlet distortion, these methods were judged to be as good as any other that could be easily used with the available data. Weight flow was measured by the calibrated venturi flow nozzles in the discharge lines and was corrected by a $\sqrt{\theta}/\delta$ term obtained from the average inlet conditions at plane 0.65.

Stall Testing. The initial stall at each speed was performed to determine the stall limit and the general nature of the rotating stall cells. The discharge throttle valve was closed slowly until strain gage and hot-wire anemometer signals indicated that rotating stall cells had formed in the rotor. Three shielded hot-wire anemometers were immersed to the 10%, 50% and 90% positions at plane 1.54, and oscillograph traces were obtained which showed the radial extent of the stalled region. The stalls were cleared as soon as possible after their appearance. The throttle valve was then reset to a position as close as possible to the stall limit, and an overall performance data point was recorded.

Near the end of each test run, if rotor blade stresses were considered to be low enough, the vehicle was stalled a second time at each speed. Conditions were stabilized in the stalled mode of operation, and a rotating-stall overall performance data point was recorded. When this was completed, speed was maintained and the discharge throttle valve was opened slowly until the stall cleared; at this condition a stall-removal overall performance data point was recorded. During this final stall testing, the three hot-wire anemometers were immersed to the position where the rotating stall cells had been most severe in the initial stall testing. The resulting oscillograph traces provided information from which the number and rotative speed of the stall cells could be determined using the methods described in reference 4.

The discharge throttle valve was geared for a fast opening-closing rate during the initial stall testing and was closed in a stepwise fashion by the operator. The discharge valve was geared to move very slowly during the rotating-stall and stall-removal testing. It was then actuated at a constant rate so that the stall line would be obtained in a fully consistent manner.

An ICPAC* trace was obtained whenever the vehicle was stalled, and the approx-

* Instantaneous Compressor Performance Analysis Computer. This is an analogue circuit which senses weight flow and pressure ratio, and plots these quantities nearly instantaneously to provide an approximate on-line compressor performance map.

proximate stalling weight flow was obtained by recording the ICPAC flow at the instant stall was detected. The true stalling weight flow was obtained from a correlation of ICPAC flow versus actual weight flow using values obtained during overall performance testing. The total-pressure ratio at stall was obtained by extrapolating the speed line on the performance map using the ICPAC trace as a guide. The ICPAC traces also indicated the nature of the hysteresis involved in throttling into and out of stall.

Screen Rotation Tests. The circumferential and radial variations of the flow at rotor inlet and discharge were investigated in considerable detail during tests with the heavy 90° circumferential distortion screen in place. The screen was set so that its centerline was in a known position relative to top center, and rotor speed and throttle valve positions were set to the desired values. When conditions were stabilized, an overall performance data point was recorded. At the same time, two angle-seeking cobra probes at plane 0.90 and two at plane 1.54 were immersed to the 10%, 50% and 90% positions, and their nulled flow angle readings were recorded. Three throttle valve settings at 100% rotor speed and one at 90% speed were investigated in this manner for each of 15 screen positions, and a more limited amount of data was obtained at one additional throttle setting at 100% speed. No rotating-stall or stall-removal overall performance data points were recorded, nor were hot-wire anemometer data obtained. Unstalled overall performance was processed in the same manner as in other testing.

## RESULTS AND DISCUSSION

The testing reported herein was conducted on the plain casing insert configuration with various types of inlet flow distortions. The basic performance of this rotor with undistorted inlet flow is documented in reference 4. The performance obtained with five different distorted inlet flow conditions is presented and discussed in the following sections.

### Radial Distortion Testing

The screen used to produce the tip radial inlet distortion pattern is shown in figure 4 (a). This screen covered the outer 40% of the inlet annulus area at plane 0.10. Two of the five elements on each inlet distortion total-pressure rake were thus located in the region of distorted inlet flow.

Overall Performance. A tabulation of all overall performance data points taken during radial distortion testing is given in table 1 (a), and the compressor performance map based on these data is shown in figure 5. Rotating stalls were encountered early in this test while accelerating with the discharge throttle valve wide open. The outlet guide vanes were then reset to decrease incidence angle by 10°. This reduced system losses and allowed more flow to be passed at wide open throttle. This adjustment eliminated the stall problem, and all data presented in table 1 (a) and figure 5 thus were obtained with the reset OGV. A similar adjustment of the OGV was made during radial distortion testing with the bleed insert configuration, reference 6. It was determined in that earlier test that the OGV setting had no effect on overall performance or on the stall point.

The dashed lines on the performance map (figure 5) represent performance with undistorted inlet flow as reported in reference 4. There is a significant reduction in adiabatic efficiency due to radial inlet distortion, but at 70% and 90% speeds the total-pressure ratio at a given weight flow is higher than in undistorted inlet testing. These same results were observed in previous radial distortion tests (references 5 and 6), and are believed to be characteristic of this rotor.

Figure 6 presents plots of inlet and discharge total pressures and discharge total temperature for Reading 45, a data point at 100% speed near stall. At this operating condition the severity of the distortion pattern at plane 0.65, the inlet measuring station, is indicated by the value of the distortion parameter $(P_{max} - P_{min})/P_{max}$ equal to about 0.18. The average total pressures in the distorted and undistorted regions were used to obtain the above value.

Stall Performance. The radial distortion stall line shown on the performance map (figure 5) is based on the stall testing in which the slow-acting discharge throttle valve was used. The stalling weight flow and total-pressure ratio were obtained as discussed in the Test Procedure Section. The stall points were quite repeatable, and were not affected by the adjustment made in outlet guide vane setting angle.

The overall performance data points recorded while operating with rotating stalls present in the rotor are shown as solid symbols in figure 5. These rotating-stall data points are also identified in table 1 (a) by the abbreviation (RS) next to the reading number. The accuracy of these data is questionable due to the unsteadiness of the flow, but they do indicate the substantial performance loss caused by rotating stall. The rotating stalls would not clear unless speed was reduced, so it was impossible to obtain stall-removal overall performance data with this inlet condition.

Rotating stalls were encountered at all speeds. For the first stall at each speed, the shielded hot-wire anemometers were immersed to 10%, 50% and 90% of the annulus height at plane 1.54 behind the rotor. The traces obtained indicated that the rotating stall cells were most severe at the tip and were very weak at the pitchline and the hub in all instances. The same type of stall trace was observed in previous radial distortion testing (references 5 and 6), and again indicates that rotating stall initiates at the rotor tip. During the rotating-stall testing the hot wire anemometers were placed at the 10% immersion. The number and rotative speed of the stall cells calculated from the resulting traces are listed in table 2.

## Heavy 90° Circumferential Distortion Testing

The distortion screen used in this test sequence is shown in figure 4 (b). It covered a 90° arc of the inlet annulus area at plane 0.10, and was located with its centerline at 180° from top center during overall performance testing. The inlet distortion total-pressure rake located at 196° was therefore in the region of distorted inlet flow. The distortion screen was later rotated to fifteen positions relative to the instrumentation in order to obtain surveys of inlet and discharge flow conditions.

Overall Performance. Figure 7 presents the compressor performance map for the heavy 90° circumferential inlet distortion condition. The dashed lines on this figure represent performance with undistorted inlet flow as reported in reference 4. A tabulation of overall performance data points recorded during tests with this inlet condition is given in table 1 (b). All data presented in figure 7 and listed in table 1 (b) were obtained with the distortion screen in the nominal position of 180° from top center.

The compressor performance map, figure 7, shows that large reductions in weight flow, total-pressure ratio and adiabatic efficiency result when this rotor is subjected to this heavy 90° circumferential inlet flow distortion. A value for the distortion parameter $(P_{max} - P_{min})/P_{max}$ equal to 0.14 was calculated near stall at 100% speed. These results are very similar to those obtained in previous tests with the same inlet distortion pattern (references 5 and 6).

Stall Performance. Rotating stalls were observed at all speeds, but high rotor stresses were observed at 100% speed which made it inadvisable to record data in stall at that speed. Rotating-stall and stall-removal data were obtained at 70% and 90% design speed and are identified by solid and half-shaded symbols, on the performance map (figure 7) and by the abbreviations (RS) and (SR) next to the reading number in table 1 (b). The 70% and 90% speed stalling weight flows and total-pressure ratios shown in figure 7 were determined from ICPAC system data obtained during rotating-stall testing, and the stall point at 100% speed is based on preliminary stall testing. Stalling weight flow was repeatable to within plus or minus 1.0 lb/sec.

Hot wire anemometer traces obtained during stalls were similar to those from earlier circumferential distortion testing, in that the stall cells were about the same strength at the tip and pitch but were very weak at the hub. The number and rotative speed of the stall cells calculated from these traces are listed in table 2. From these results it is believed that the rotating stalls initiate at the tip of the rotor blade and that the hub is essentially free of stall. The unusual stall line of this rotor with circumferential inlet distortion, in which the reduction in stalling weight flow was so large that unstalled range of operation increased despite a loss in total-pressure ratio, is seen in figure 7. The screen rotation tests described in the next section, in which circumferential surveys of flow conditions were obtained, were performed in order to obtain a better understanding of this unusual stall performance.

Circumferential Surveys. Circumferential surveys of flow conditions were obtained at several operating points by rotating the inlet distortion screen past the instrumentation in the manner described in the Test Procedure Section. Overall performance data obtained during screen rotation tests with the screen at the standard bottom center position agreed reasonably well with corresponding data obtained during the standard overall performance testing. Figures 8 - 12 present the results of this testing as distributions of inlet and discharge pressures and flow angles plus discharge total temperatures. Because the very large quantity of data generated could not be plotted conveniently, these figures present only smooth curves which represent the average of the data points. Scatter in the data was normally very small, except possibly for discharge static pressures which had a spread of about ± 0.5 psia.

In figures 8 - 12 the static pressures were obtained from wall taps. Only the pitchline inlet total pressure has been plotted because the radial variations of this property was very small, and the pitchline data was the most representative. All pressures plotted in these figures are uncorrected values because the correction factor S normally used in the data reduction computer program varied as the distortion screen was moved relative to the inlet total-pressure rakes. Since ambient pressures varied only between 14.60 to 14.77 psia during the tests, the use of uncorrected pressures is not believed to have impaired the accuracy of the figures.

The flow angle data in figure 8 are incomplete because the rotor began encountering rotating stalls during screen rotation tests at 100% design speed with the discharge value set to 10.0. This operating point lies within a region of intermittent stall as shown in the performance map, figure 7. The stall point of the rotor appears to be very sensitive to slight disturbances in this region. Although overall performance data had been recorded there earlier, the presence of traverse probes in the stream and other-than-standard screen positions were enough to cause stall to occur.

One noticeable feature of these data is the existence of large negative flow angles (counter to rotor rotation) at the inlet, resulting in high incidence angles in the region 160° to 240° from top center. This produces very high total temperatures in a corresponding region of the discharge annulus. Discharge flow angles are high and discharge total pressures are low in this region at tip and pitch, but the hub has moderate flow angles and high total pressures. These trends exist at all speeds and flows investigated, and indicate that part of the flow is stalled all the time in the outer part of the rotor but not at the hub. This stalled region acts as a blockage in the flow field and reduces the aerodynamic loading of the rotor outside this region. Apparently because of this reduced loading in the rest of the annulus, the stalled region is unable to propagate as a rotating stall until weight flow is reduced well below the stalling value for undistorted inlet flow. It is significant to note in figure 8 that a top center (zero degrees), outside the stalled region the tip discharge total-temperature ratio is 1.15; this value is very close to the maximum tip total-temperature ratio of 1.17 with radial distortion (figure 6) and virtually identical to the maximum tip total-temperature ratio with undistorted inlet flow (reference 4). It thus appears that with circumferential inlet distortion, rotating stall does not appear until the undistorted part of the annulus reaches aerodynamic loadings where rotating stall cells normally appear.

## Additional Circumferential Distortion Testing

Three other circumferential inlet distortion overall performance tests were conducted on the plain casing insert configuration: a light 90° pattern, a light 180° pattern, and a rounded 120° pattern. The design of these screens is discussed under Apparatus and Procedure, and photos of the screens appear as figures 4 (c) - 4 (e). The screens were placed with their centerlines at 180°, 150° and 196° respectively so as to be in the proper relationship to the inlet distortion total-pressure rakes.

Overall Performance. Compressor performance maps for the three additional circumferential distortion conditions are presented in figures 13, 14 and 15, and tabulations of overall performance are given in tables 1 (c), 1 (d) and 1 (e). Dashed lines on the performance maps represent undistorted inlet performance for the plain casing insert configuration (refernce 4). Values of the distortion parameter $(P_{max} - P_{min}) / P_{max}$ were calculated for the overall performance data point nearest stall at 100% speed in each of these three circumferential distortion tests. These values were 0.07 for the light 90° pattern, 0.08 for the light 180° pattern, and 0.13 for the rounded 120° pattern. Average inlet pressures in the distorted and undistorted regions were used to obtain these values.

Figures 16, 17 and 18 show circumferential variations of inlet pressures, discharge pressures and discharge total temperature for the above mentioned 100% speed data points nearest stall. The curves through the data on these figures were drawn using the trend of the screen rotation test results (figures 8 - 12) as a guide. Although only a limited amount of data was available for use in figures 16 - 18, these plots do suggest that a stable stalled zone exists at the rotor tip and pitch behind the distortion screen with these three inlet distortions, similar to that discussed in screen rotation tests with the heavy 90° circumferential pattern. The effect of this stalled zone in relieving the aerodynamic loading in the rest of the annulus can again be seen.

Stall Performance. Strain gage and hot wire anemometer signals showed that rotating stalls occurred at all speeds in each of the three additional circumferential inlet distortion tests. High rotor blades stress levels prevented rotating-stall and stall-removal overall performance data from being obtained at the higher speeds. Those data which were obtained are indicated by solid and half-shaded symbols respectively on the performance maps (figures 13-15) and by the abbreviations (RS) and (SR) next to the reading numbers in tables 1 (c), 1 (d) and 1 (e).

Traces from the hot wire anemometers obtained during stalls showed that at all speeds with each inlet distortion the rotating stall cells extended over most of the span of the rotor blades, but were most severe at the tip and quite weak at the hub. The stall generally cleared as soon as the discharge throttle valve was opened, there being rather little hysteresis involved in the process of throttling into and out of the stalled mode of operation. In several instances, the number of rotating stall cells was seen to change while operating in stall with no changes having been made in operating conditions. The number and rotative speed of the stall cells, when available, are listed in table 2.

The stall performance for the two light circumferential distortions (figures 13 and 14) are quite similar. Both distortions produced essentially the same stall points, with stall margin at 100% design speed slightly less than with undistorted inlet flow but improved at lower speeds. The 120° rounded distortion pattern produced stall performance (figure 15) which was very similar to that produced by the heavy 90° pattern. Both the 120° rounded and the heavy 90° distortions had the same maximum distortion severity, and both showed improved stall margin at all speeds relative to the undistorted inlet flow stall line. These results indicate that in this rotor the stall margin with circumferential inlet distortion is determined primarily by the severity of the distortion rather than by the shape or extent of the pattern.

## REFERENCES


1. Kussoy, Marvin I., and Bachkin, Daniel: Comparison of Performance of Two Aerodynamically Similar 14-Inch Diameter Single Stage Compressor Rotors of Different Chord Length, NACA RM E57I03, 1958.

2. Swan, W. C.: An Experiment with Aspect Ratio as a Means of Extending the Useful Range of a Transonic Inlet Stage of an Axial Flow Compressor, Journal of Engineering for Power, Trans. ASME, Series A, Vol. 88, 1966, pp. 1 - 12.

3. Giffin, R. G. and Smith, L.H., Jr.: Experimental Evaluation of Outer Case Blowing or Bleeding of Single Stage Axial Flow Compressor, Part 1 - Design of Rotor and Bleeding and Blowing Configurations, NASA CR-54587, 1966.

4. Koch, C. C. and Smith, L.H., Jr.: Experimental Evaluation of Outer Case Blowing or Bleeding of Single Stage Axial Flow Compressor, Part II - Performance of Plain Casing Insert Configuration with Undistorted Inlet Flow and Boundary Layer Trip, NASA CR-54588, 1968.

5. Koch, C. C. and Smith, L.H., Jr.: Experimental Evaluation of Outer Case Blowing or Bleeding of Single Stage Axial Flow Compressor, Part III - Performance of Blowing Insert Configuration No. 1, NASA CR-54589, 1968.

6. Koch, C. C. and Smith, L. H., Jr.: Experimental Evaluation of Outer Case Blowing or Bleeding of Single Stage Axial Flow Compressor, Part IV - Performance of Bleed Insert Configuration No. 3, NASA CR-54590, 1968.

TABLE 1 (a) - OVERALL PERFORMANCE FOR RADIAL INLET DISTORTION TESTING

| Reading | Total Pressure Ratio | Rotor Adiabatic Efficiency | Inlet Corrected Flow lbs/sec | Corrected Speed % Design | Throttle Valve Setting |
|---|---|---|---|---|---|
| 38 | 1.370 | .815 | 183.2 | 100.15 | 32.0 |
| 39 | 1.360 | .812 | 184.3 | 100.05 | 40.0 |
| 40 | 1.348 | .803 | 185.2 | 100.07 | 60.0 |
| 41 | 1.314 | .880 | 178.7 | 90.15 | 60.0 |
| 42 | 1.321 | .886 | 177.6 | 90.14 | 40.0 |
| 43 | 1.331 | .899 | 177.0 | 90.09 | 32.0 |
| 44 | 1.341 | .903 | 175.5 | 90.14 | 26.5 |
| 45 | 1.390 | .831 | 181.0 | 100.09 | 23.5 |
| 46 | 1.195 | .930 | 144.1 | 70.09 | 50.0 |
| 47 | 1.195 | .912 | 143.0 | 70.11 | 40.0 |
| 48 | 1.196 | .924 | 140.4 | 70.13 | 30.0 |
| 49 | 1.195 | .913 | 137.1 | 70.10 | 24.5 |
| 52 (RS) | 1.180 | .822 | 128.8 | 70.16 | 24.3 |
| 53 (RS) | 1.285 | .757 | 155.0 | 90.19 | 27.5 |
| 54 (RS) | 1.348 | .731 | 166.5 | 100.26 | 23.3 |

(RS) indicates a rotating-stall overall performance reading.

TABLE 1 (b) - OVERALL PERFORMANCE FOR HEAVY 90° CIRCUMFERENTIAL INLET DISTORTION TESTING

| Reading | Total Pressure Ratio | Rotor Adiabatic Efficiency | Inlet Corrected Flow lbs/sec | Corrected Speed % Design | Throttle Valve Setting |
|---|---|---|---|---|---|
| 1 | 1.187 | .755 | 110.3 | 70.14 | 8.0 |
| 2 | 1.319 | .737 | 140.7 | 90.14 | 9.0 |
| 3 | 1.393 | .702 | 148.0 | 100.21 | 8.0 |
| 9 | 1.179 | .808 | 124.0 | 70.09 | 16.0 |
| 10 | 1.183 | .784 | 118.2 | 70.09 | 12.0 |
| 11 | 1.177 | .818 | 127.5 | 70.11 | 20.0 |
| 12 | 1.166 | .805 | 137.4 | 70.13 | 50.0 |
| 13 | 1.279 | .787 | 166.1 | 90.20 | 50.0 |
| 14 | 1.306 | .785 | 155.3 | 90.13 | 17.0 |
| 15 | 1.311 | .766 | 151.0 | 90.16 | 14.0 |
| 16 | 1.315 | .755 | 147.0 | 90.20 | 12.0 |
| 17 | 1.365 | .734 | 165.9 | 100.20 | 18.0 |
| 18 | 1.380 | .719 | 158.6 | 100.14 | 12.5 |
| 19 | 1.388 | .713 | 153.5 | 100.17 | 10.0 |
| 20 | 1.332 | .740 | 174.0 | 100.16 | 50.0 |
| 21 (RS) | 1.165 | .699 | 100.8 | 70.06 | 7.2 |
| 22 (SR) | 1.186 | .772 | 110.4 | 70.12 | 8.2 |
| 23 (RS) | 1.273 | .653 | 127.7 | 90.12 | 7.9 |
| 24 (SR) | 1.318 | .745 | 141.4 | 90.10 | 9.5 |

TABLE 1 (b) - OVERALL PERFORMANCE FOR HEAVY 90° CIRCUMFERENTIAL INLET DISTORTION TESTING (CONT'D)

| Reading | Total Pressure Ratio | Rotor Adiabatic Efficiency | Inlet Corrected Flow lbs/sec | Corrected Speed % Design | Throttle Valve Setting |
|---|---|---|---|---|---|
| (The following readings were taken during screen rotation tests with the distortion screen in the standard bottom center position.) | | | | | |
| 1 | 1.324 | .753 | 140.4 | 90.03 | 9.0 |
| 2 | 1.372 | .744 | 167.5 | 99.82 | 18.0 |
| 3 | 1.396 | .733 | 154.5 | 99.86 | 10.0 |
| 51 | 1.348 | .760 | 174.8 | 99.97 | 30.0 |
| 52 | 1.387 | .735 | 157.8 | 99.87 | 11.0 |

(RS) indicates a rotating-stall overall performance reading.
(SR) indicates a stall-removal overall performance reading.

TABLE 1 (c) - OVERALL PERFORMANCE FOR LIGHT 90° CIRCUMFERENTIAL DISTORTION TESTING

| Reading | Total Pressure Ratio | Rotor Adiabatic Efficiency | Inlet Corrected Flow lbs/sec | Corrected Speed % Design | Throttle Valve Setting |
|---|---|---|---|---|---|
| 55 | 1.198 | .819 | 113.7 | 70.16 | 6.5 |
| 56 | 1.347 | .832 | 150.4 | 89.98 | 8.0 |
| 57 | 1.423 | .834 | 175.9 | 99.94 | 10.5 |
| 58 | 1.336 | .825 | 188.5 | 100.05 | 50.0 |
| 59 | 1.378 | .846 | 186.1 | 100.05 | 20.0 |
| 60 | 1.399 | .852 | 183.2 | 100.03 | 15.0 |
| 61 | 1.413 | .842 | 179.7 | 100.02 | 12.5 |
| 62 | 1.282 | .877 | 180.8 | 90.06 | 50.0 |
| 63 | 1.318 | .887 | 175.5 | 90.08 | 20.0 |
| 64 | 1.340 | .865 | 165.0 | 90.03 | 12.0 |
| 65 | 1.348 | .851 | 156.4 | 89.94 | 9.5 |
| 66 | 1.165 | .906 | 148.8 | 69.97 | 50.0 |
| 67 | 1.180 | .905 | 139.1 | 70.01 | 20.0 |
| 68 | 1.190 | .886 | 129.1 | 70.00 | 12.0 |
| 69 | 1.196 | .862 | 120.3 | 70.03 | 8.5 |
| 70 | 1.198 | .825 | 113.3 | 70.01 | 6.5 |
| 71 (RS) | 1.175 | .739 | 105.6 | 69.97 | 5.9 |
| 72 (SR) | 1.197 | .828 | 114.5 | 69.99 | 6.8 |
| 73 (RS) | 1.294 | .707 | 137.7 | 89.99 | 7.4 |
| 74 (SR) | 1.348 | .849 | 155.3 | 89.95 | 9.2 |

(RS) indicates a rotating-stall overall performance reading.
(SR) indicates a stall-removal overall performance reading.

TABLE 1 (d) - OVERALL PERFORMANCE FOR LIGHT 180° CIRCUMFERENTIAL INLET DISTORTION

| Reading | Total Pressure Ratio | Rotor Adiabatic Efficiency | Inlet Corrected Flow lbs/sec | Corrected Speed % Design | Throttle Valve Setting |
|---|---|---|---|---|---|
| 69 | 1.172 | .935 | 145.4 | 70.02 | 40.0 |
| 70 | 1.192 | .881 | 125.2 | 70.06 | 12.5 |
| 71 | 1.196 | .824 | 111.7 | 69.99 | 7.7 |
| 72 | 1.304 | .923 | 177.1 | 89.96 | 30.0 |
| 73 | 1.341 | .873 | 157.4 | 89.91 | 12.5 |
| 74 | 1.340 | .833 | 146.6 | 89.98 | 9.7 |
| 75 | 1.364 | .873 | 186.1 | [illegible]9.93 | 30.0 |
| 76 | 1.407 | .858 | 179.4 | 100.02 | 16.0 |
| 77 | 1.417 | .835 | 172.8 | 100.08 | 13.0 |
| 78 (RS) | 1.167 | .700 | 99.1 | 70.07 | 6.6 |
| 79 (SR) | 1.197 | .821 | 111.2 | 70.05 | 7.7 |

(RS) indicates a rotating-stall overall performance reading.
(SR) indicates a stall-removal overall performance reading.

TABLE 1 (e) - OVERALL PERFORMANCE FOR ROUNDED 120° CIRCUMFERENTIAL INLET DISTORTION TESTING

| Reading | Total Pressure Ratio | Rotor Adiabatic Efficiency | Inlet Corrected Flow lbs/sec | Corrected Speed % Design | Throttle Valve Setting |
|---|---|---|---|---|---|
| 81 | 1.173 | .881 | 140.3 | 69.99 | 40.0 |
| 82 | 1.186 | .812 | 122.1 | 69.96 | 12.5 |
| 83 | 1.191 | .782 | 112.6 | 70.06 | 8.4 |
| 84 | 1.352 | .754 | 178.5 | 99.92 | 30.0 |
| 85 | 1.386 | .734 | 164.9 | 100.03 | 12.5 |
| 86 | 1.401 | .729 | 156.8 | 100.15 | 9.5 |
| 87 | 1.293 | .807 | 168.7 | 89.97 | 30.0 |
| 88 | 1.319 | .781 | 152.7 | 89.95 | 12.5 |
| 89 | 1.326 | .761 | 140.1 | 89.99 | 8.5 |
| 90 (RS) | 1.171 | .720 | 102.0 | 70.06 | 7.3 |
| 91 (SR) | 1.191 | .787 | 111.5 | 70.06 | 8.1 |

(RS) indicates a rotating-stall overall performance reading.
(SR) indicates a stall-removal overall performance reading.

TABLE 2 - TABULATION OF ROTATING STALL CELL DATA

| Corrected Speed % Design | Throttle Valve Setting | Rotating Stall Rdg. No. | Number of Stall Cells | Stall Cell Speed / Rotor Speed | Radial Extent of Stall Cells |
|---|---|---|---|---|---|
| (a) Radial Distortion | | | | | |
| 70 | 24.3 | 52 | 3 | .419 | Outer 50% |
| 90 | 27.5 | 53 | 4 | .425 | Outer 50% |
| 100 | 23.3 | 54 | 3 | .427 | Outer 50% |
| (b) Heavy 90° Circumferential Distortion | | | | | |
| 70 | 7.2 | 21 | 3 | .428 | Outer 50% + |
| 90 | 7.9 | 23 | 3 | .437 | Outer 50% + |
| 100 | 7.3 | -- | - | ---- | Outer 50% + |
| (c) Light 90° Circumferential Distortion | | | | | |
| 70 | 5.9 | 71 | 2 | .409 | Full Span |
| 90 | 7.4 | 73 | 3 | .469 | Full Span |
| 100 | 9.5 | -- | - | ---- | Full Span |
| (d) Light 180° Circumferential Distortion | | | | | |
| 70 | 6.6 | 78 | 3 | .425 | Full Span |
| 90 | 8.7 | -- | - | ---- | Full Span |
| 100 | 11.8 | -- | - | ---- | Full Span |
| (e) Rounded 120° Circumferential Distortion | | | | | |
| 70 | 7.3 | 90 | 4 | .522 | Full Span |
| 90 | 7.5 | -- | - | ---- | Full Span |
| 100 | 8.5 | -- | - | ---- | Full Span |

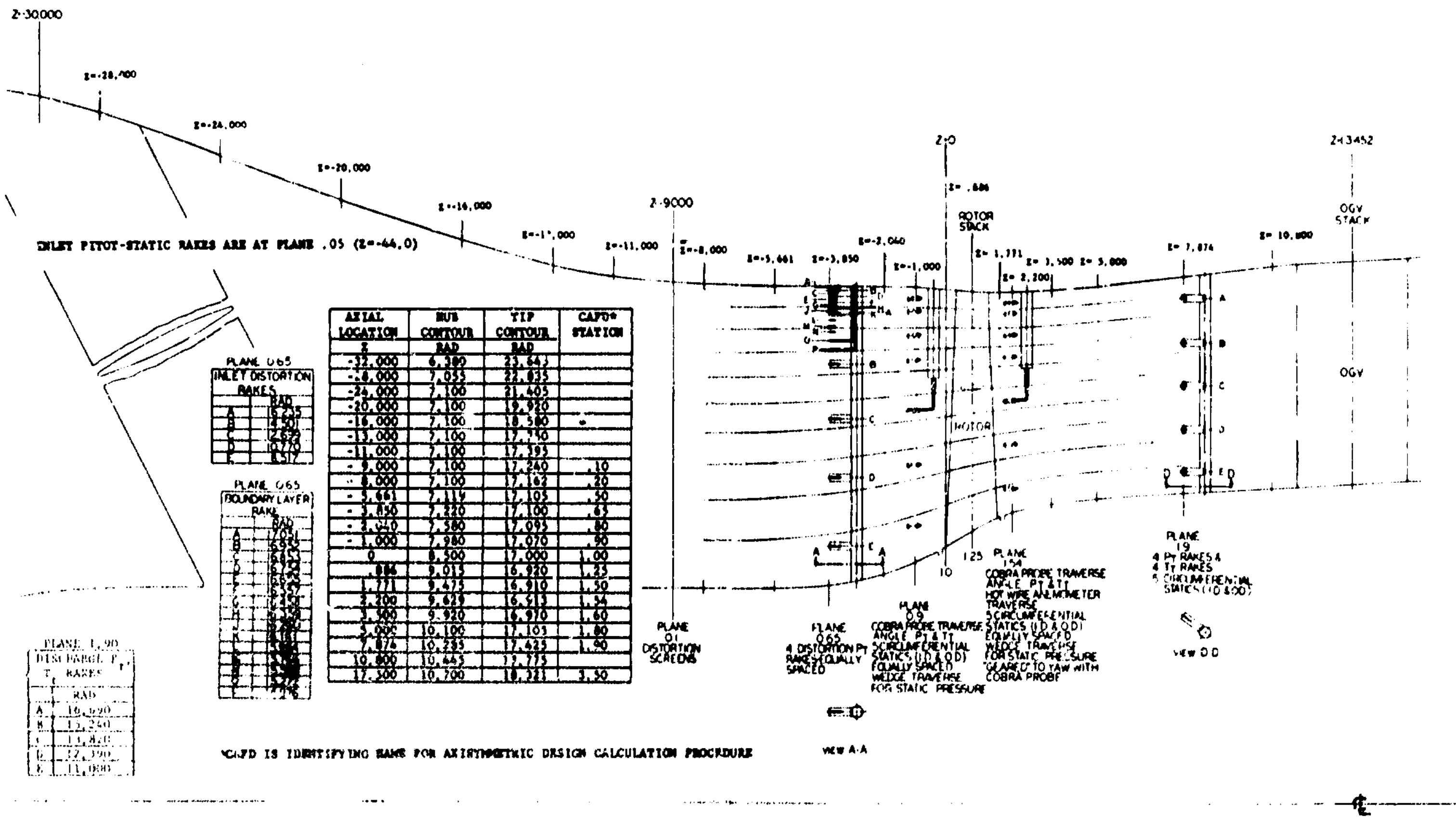


| AXIAL LOCATION Z | HUB CONTOUR RAD | TIP CONTOUR RAD | CAPD* STATION |
|---|---|---|---|
| -32,000 | 6,380 | 23,643 | |
| -28,000 | 7,055 | 22,835 | |
| -24,000 | 7,100 | 21,405 | |
| -20,000 | 7,100 | 19,920 | |
| -16,000 | 7,100 | 18,580 | * |
| -13,000 | 7,100 | 17,750 | |
| -11,000 | 7,100 | 17,395 | |
| - 9,000 | 7,100 | 17,240 | .10 |
| - 8,000 | 7,100 | 17,162 | .20 |
| - 5,661 | 7,119 | 17,105 | .50 |
| - 3,850 | 7,220 | 17,100 | .65 |
| - 2,040 | 7,580 | 17,095 | .80 |
| - 1,000 | 7,980 | 17,070 | .90 |
| 0 | 8,500 | 17,000 | 1.00 |
| .886 | 9,015 | 16,920 | 1.25 |
| 1,771 | 9,475 | 16,910 | 1.50 |
| 2,200 | 9,629 | 16,913 | 1.54 |
| 3,500 | 9,920 | 16,970 | 1.60 |
| 5,000 | 10,100 | 17,103 | 1.80 |
| 7,876 | 10,235 | 17,425 | 1.90 |
| 10,800 | 10,443 | 17,775 | |
| 17,300 | 10,700 | 18,321 | 3.50 |

Figure 1 - Meridional view showing location of instrumentation

24 INLET $T_t$ THERMOCOUPLES
DISTRIBUTED ON INLET SCREEN
24 ADDITIONAL THERMOCOUPLES
FOR IN-TEST CHECK (NOT SHOWN)

| Instrument | Qty | Plane | Circumferential Location, Deg |
|---|---|---|---|
| Inlet Pitot Static Rake | 6 | 0.05 | 30, 90, 150, 210, 270, 330 |
| Inlet Distortion $P_t$ Rake | 4 | 0.65 | 18, 106, 196, 286 |
| Inlet Boundary Layer Rake | 1 | 0.65 | 53 |
| Inlet Cobra Probe | 1 | 0.90 | 216 |
| Inlet Static Pressure Probe | 1 | 0.90 | 29 |
| Exit Cobra Probe | 1 | 1.54 | 16 |
| Exit Static Pressure Probe | 2 | 1.54 | 127, 295 |
| Hot Wire Anemometer Probe | 5 | 1.54 | 38, 66, 111, 283, 331 |
| Exit $T_t$ Rake | 4 | 1.90 | 5, 95, 197, 287 |
| Exit $P_t$ Rake | 4 | 1.90 | 17, 107, 189, 279 |

STATIC PRESSURE TAP
CIRCUMFERENTIAL LOCATIONS

| Plane 0.65 | Plane 0.90 | Plane 1.54 | Plane 1.90 | Plane 3.50 |
|---|---|---|---|---|
| CASING TAP | | | | |
| 0 | 0 | 0 | 0 | 0 |
| 20 | 72 | 72 | 72 | 72 |
| 72 | 110 | 144 | 110 | 144 |
| 110 | 144 | 216 | 144 | 216 |
| 144 | 160 | 288 | 160 | 288 |
| 160 | 180 | | 180 | 334 |
| 180 | 200 | | 200 | |
| 200 | 216 | | 216 | |
| 216 | 250 | | 250 | |
| 250 | 288 | | 300 | |
| 288 | | | | |
| HUB TAPS | | | | |
| 0 | 0 | 0 | 0 | 0 |
| 25 | 72 | 72 | 72 | 72 |
| 72 | 110 | 144 | 110 | 144 |
| 113 | 144 | 216 | 144 | 216 |
| 144 | 160 | 288 | 160 | 288 |
| 160 | 180 | | 180 | 334 |
| 180 | 200 | | 200 | |
| 203 | 216 | | 216 | |
| 216 | 250 | | 250 | |
| 250 | 288 | | 300 | |
| [illegible] | | | | |

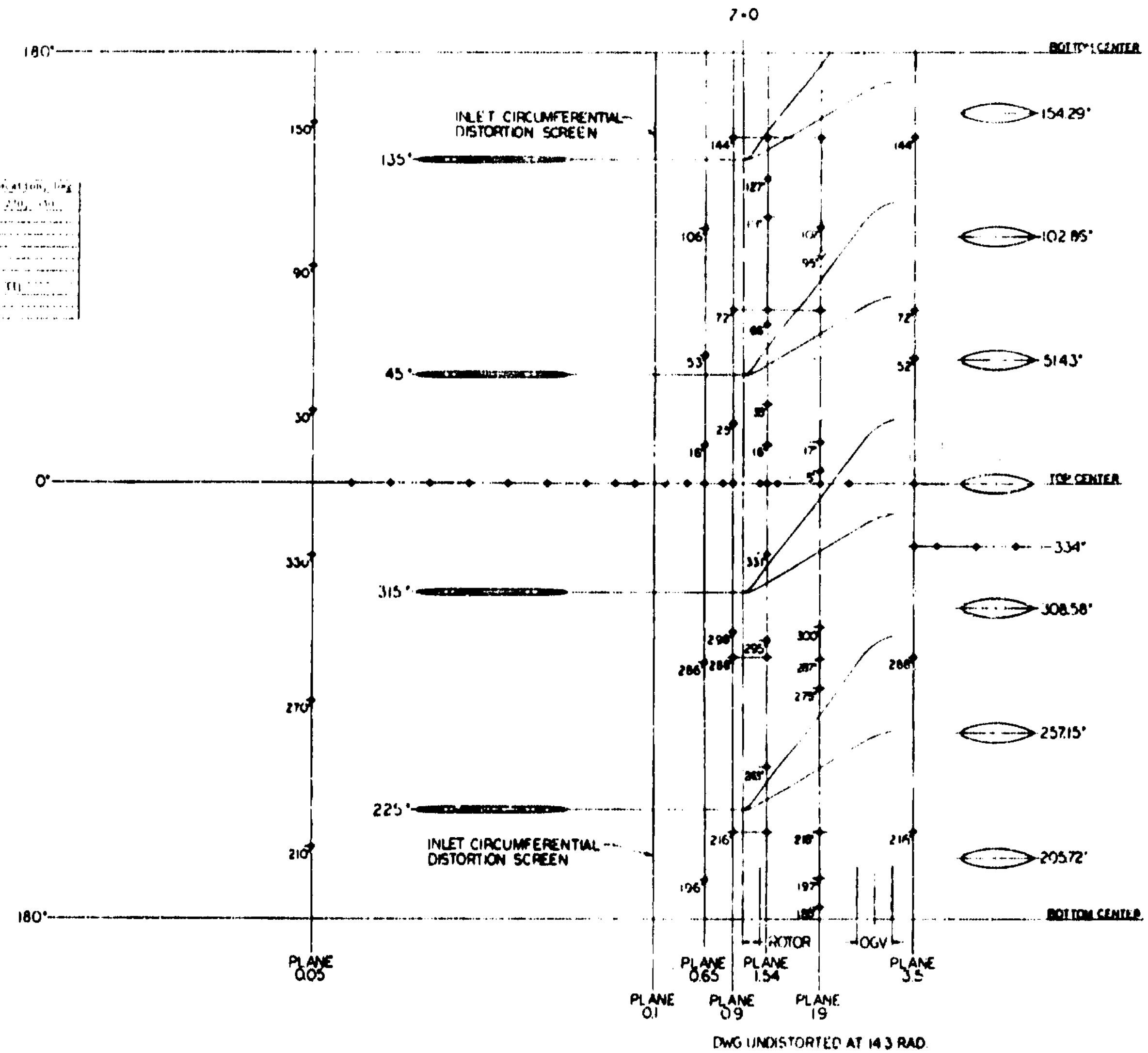


Figure 2 - Development showing circumferential location of instrumentation

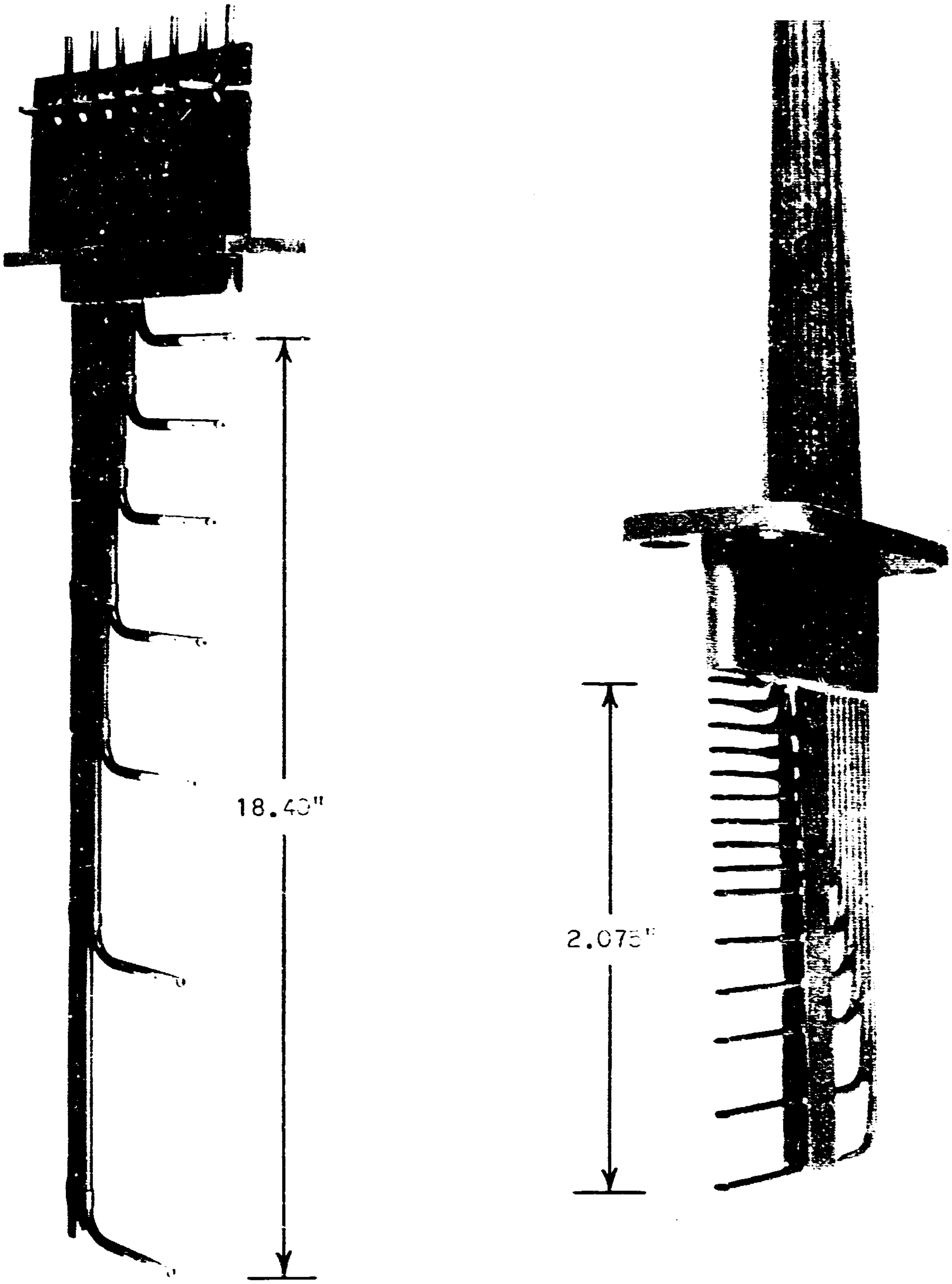

(a). - Inlet pitot-static rake. (b). - Casing boundary layer rake.

**Figure 3 - Photographs of instrumentation**

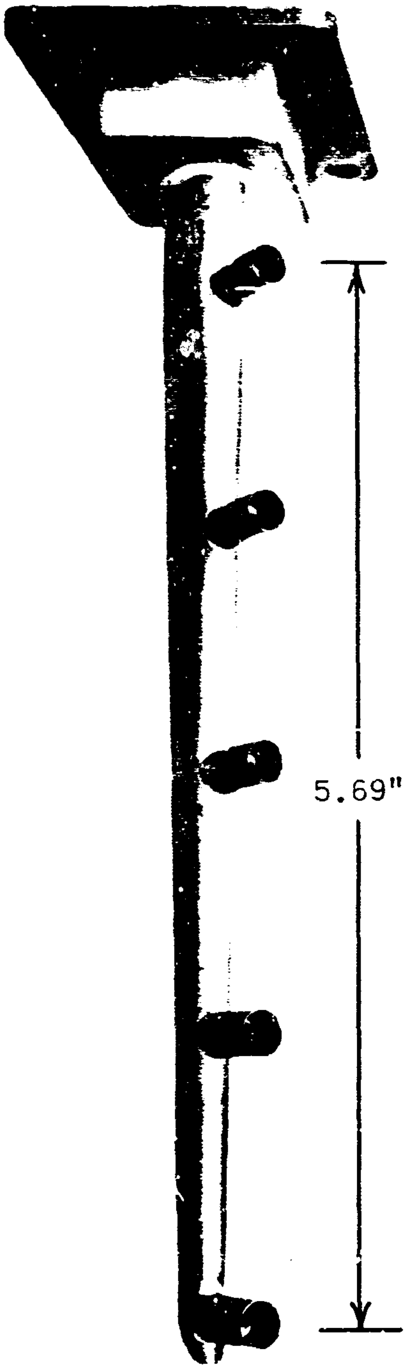


(c). - Discharge total temperature rake.

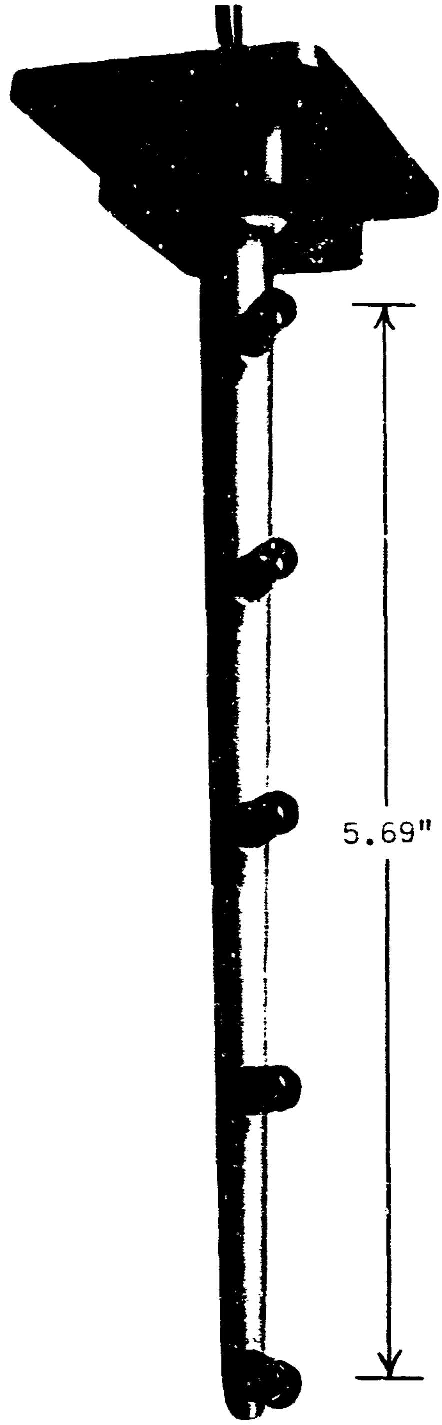


(d). - Discharge total pressure rake.

Figure 3 - Photographs of instrumentation

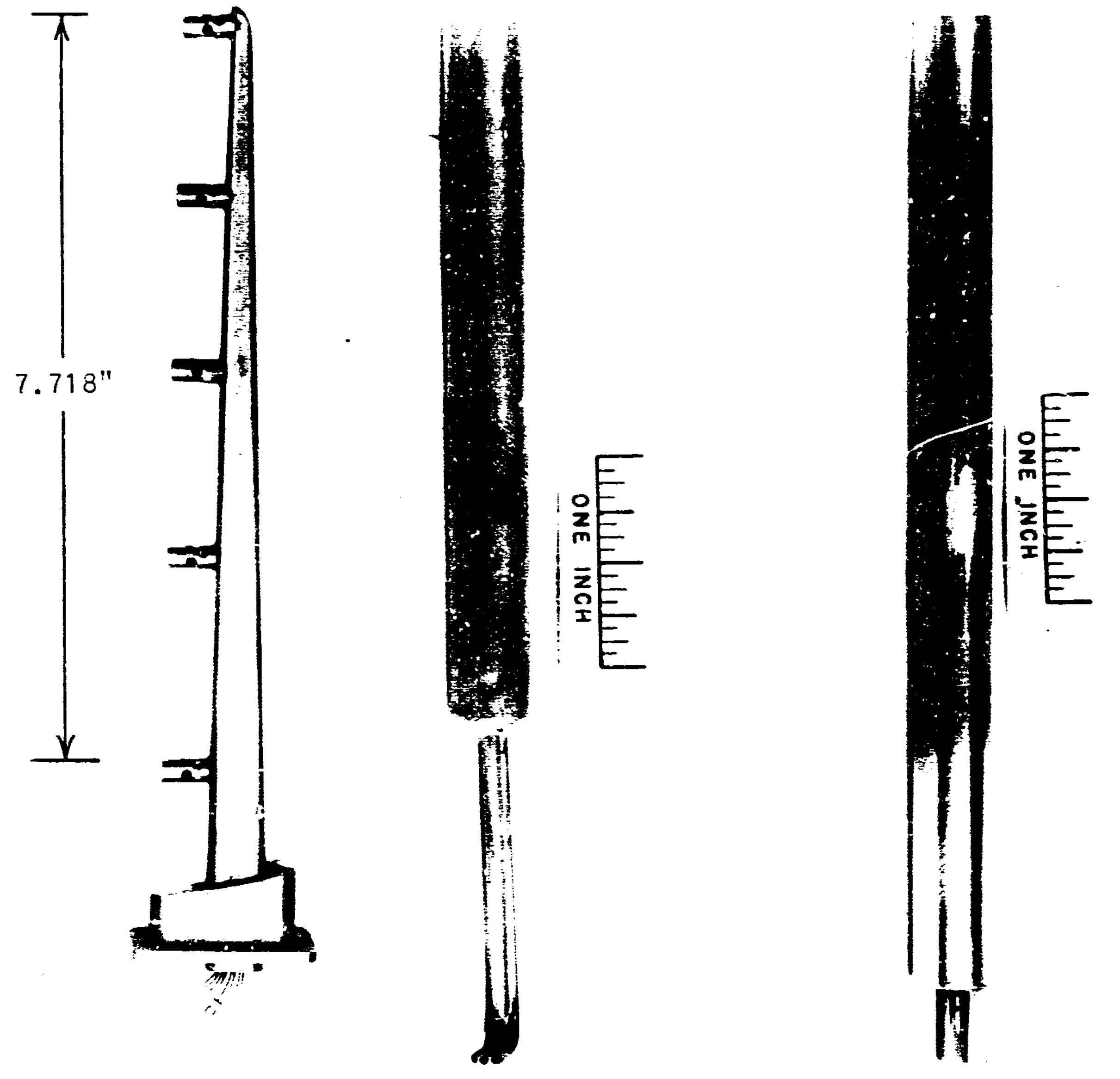


(e) - Inlet distortion total-pressure rake

(f) - Cobra probe for sensing flow angle

(g) - Shielded hot wire probe

Figure 3. - Photographs of instrumentation.

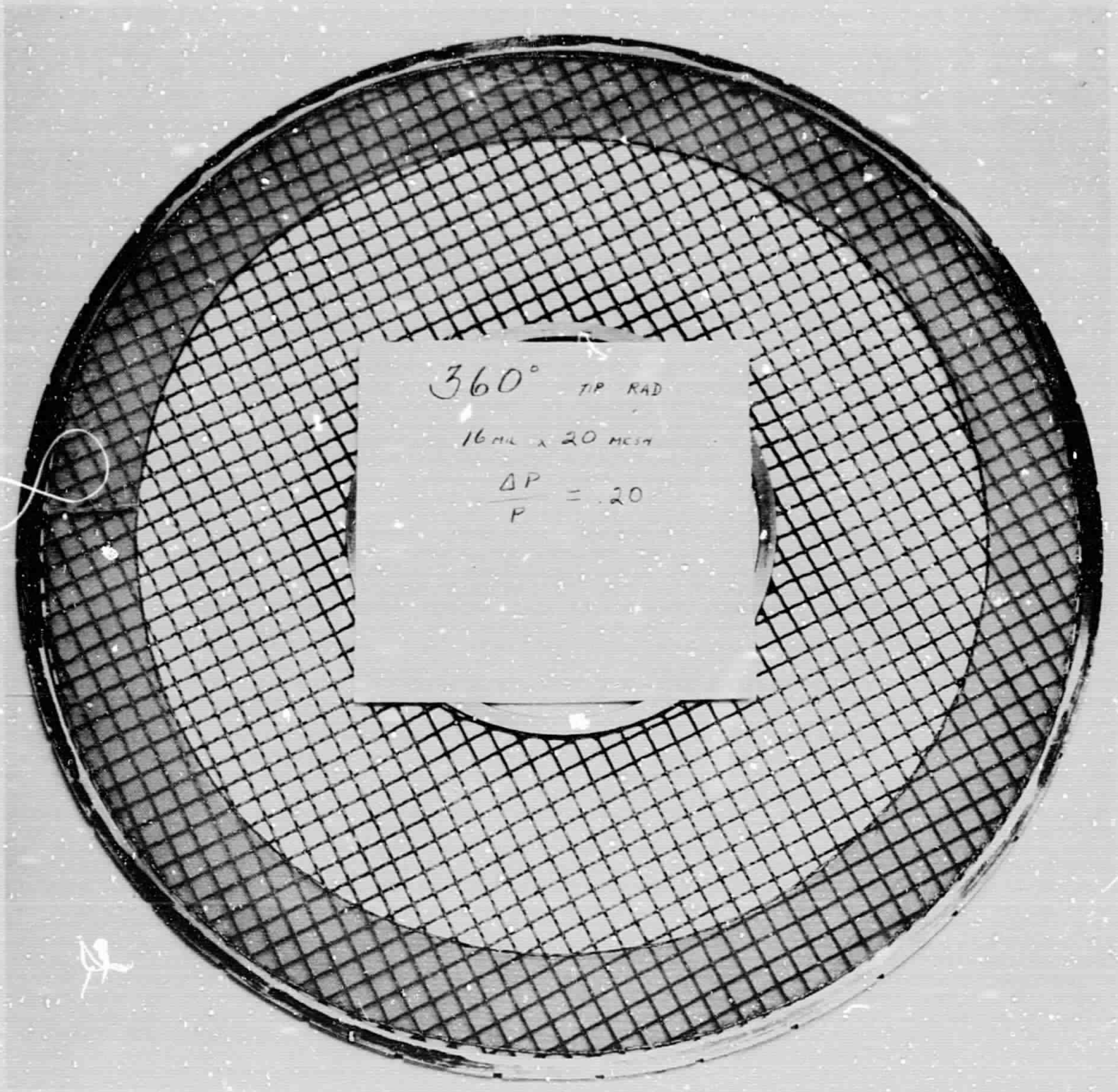


Figure 4(a) - Photograph of radial inlet distortion screen mounted on support screen


Figure 4(b) - Photograph of heavy 90° circumferential inlet distortion screen mounted on support screen

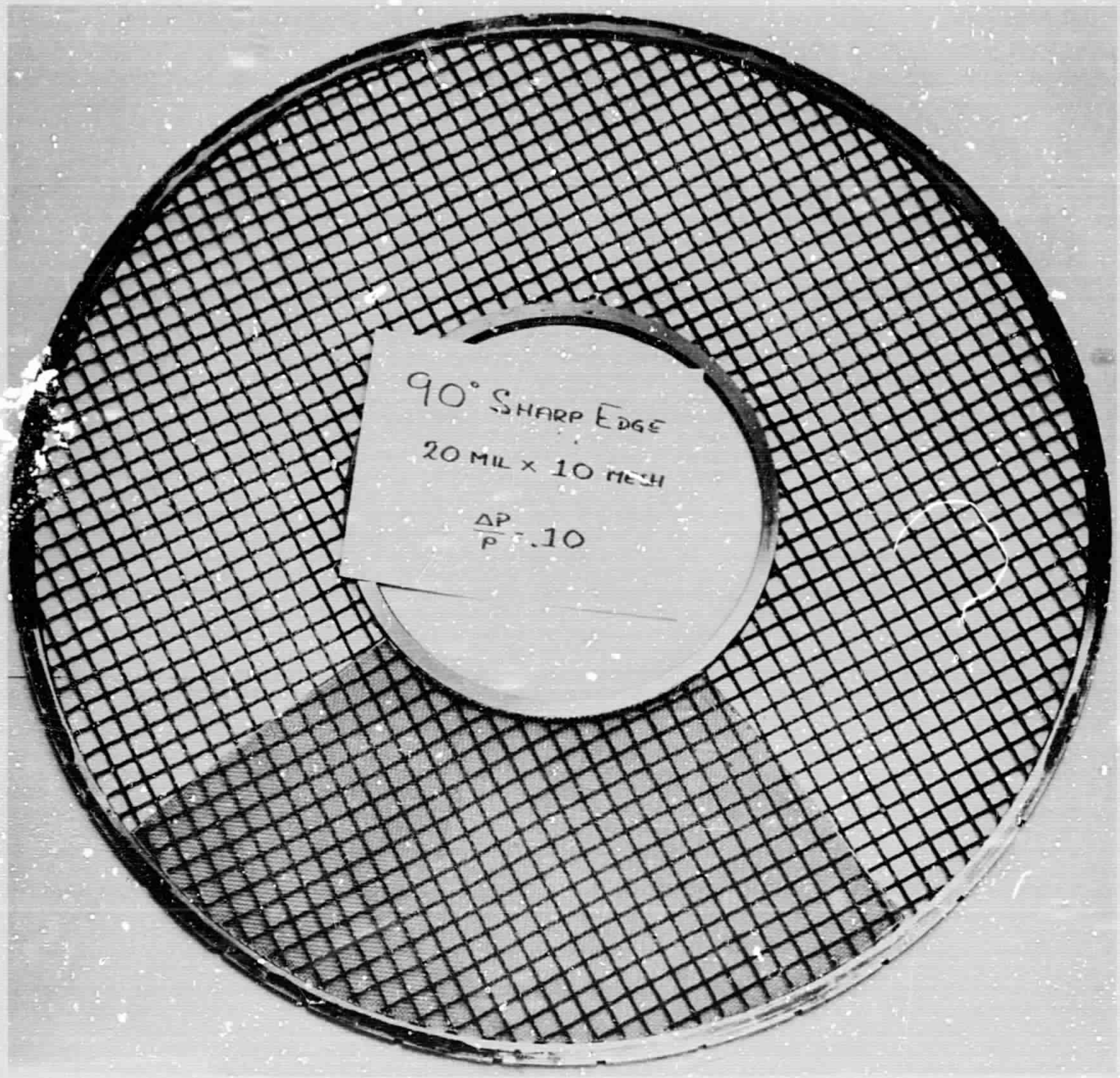


Figure 4 (c). - Photograph of light 90° circumferential inlet distortion screen mounted on support screen.

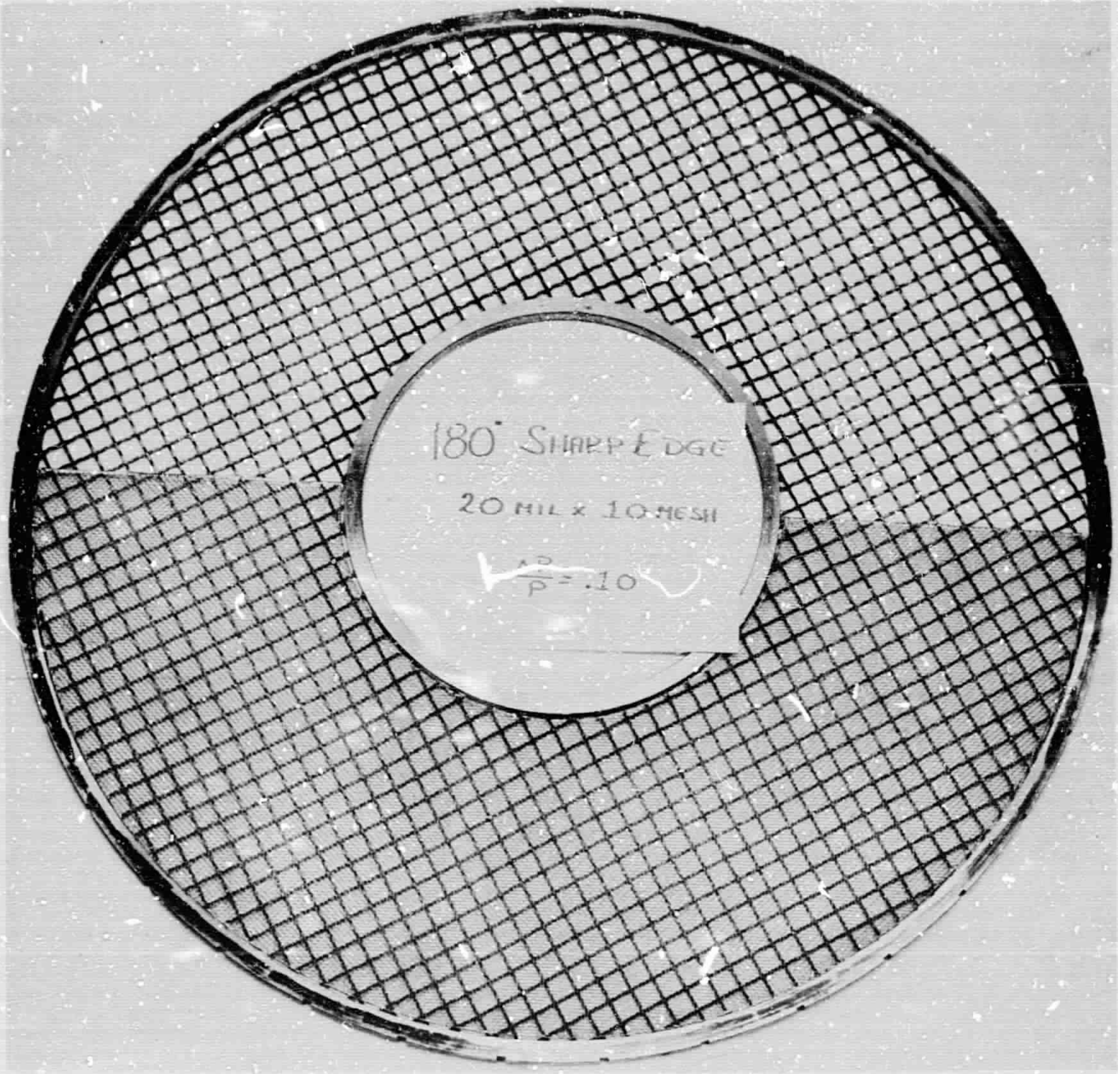


Figure 4 (d). - Photograph of light 180° circumferential inlet distortion screen mounted on support screen.

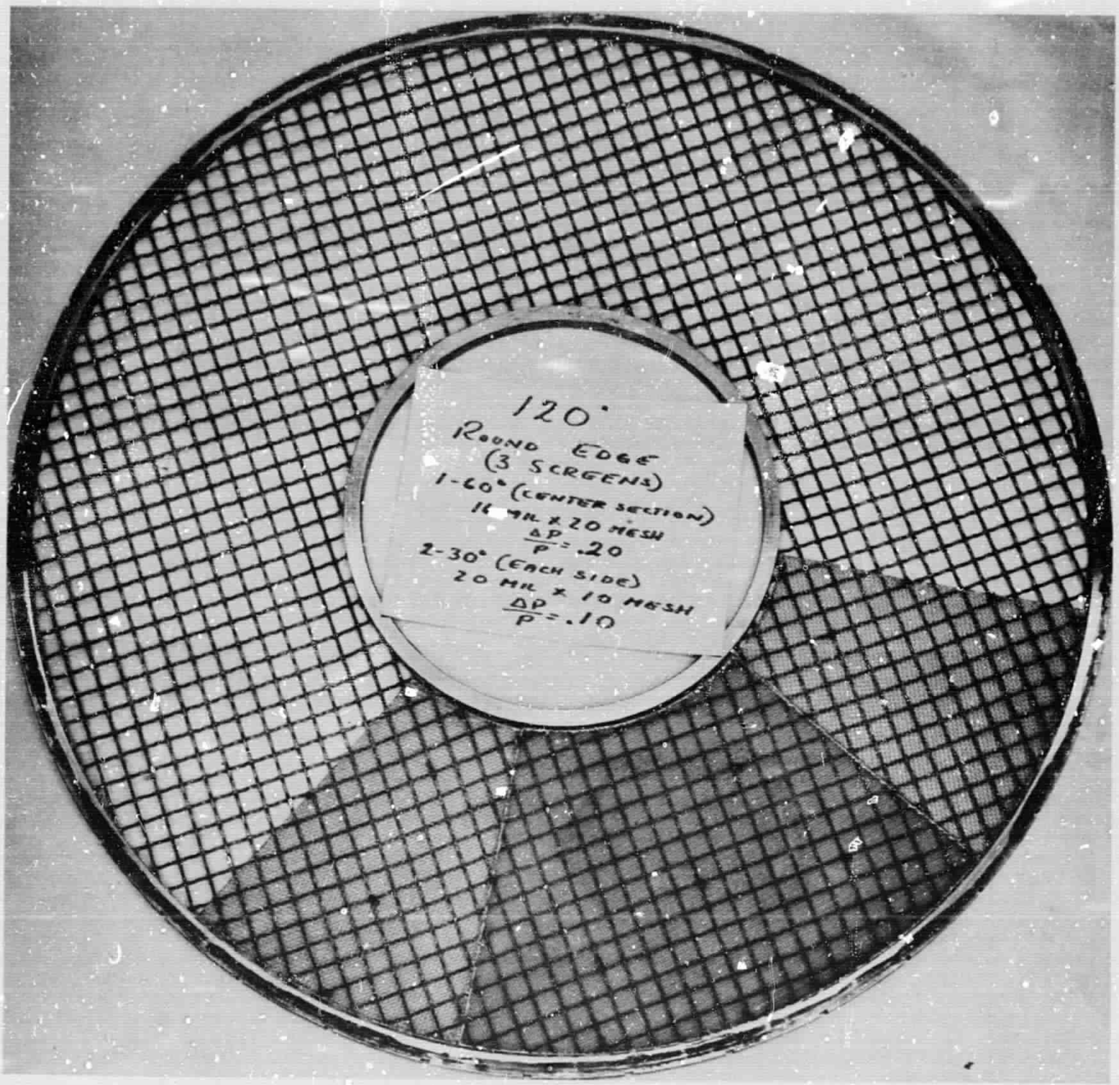


Figure 4 (e). - Photograph of rounded 120$^{\circ}$ circumferential inlet distortion screen mounted on support screen.

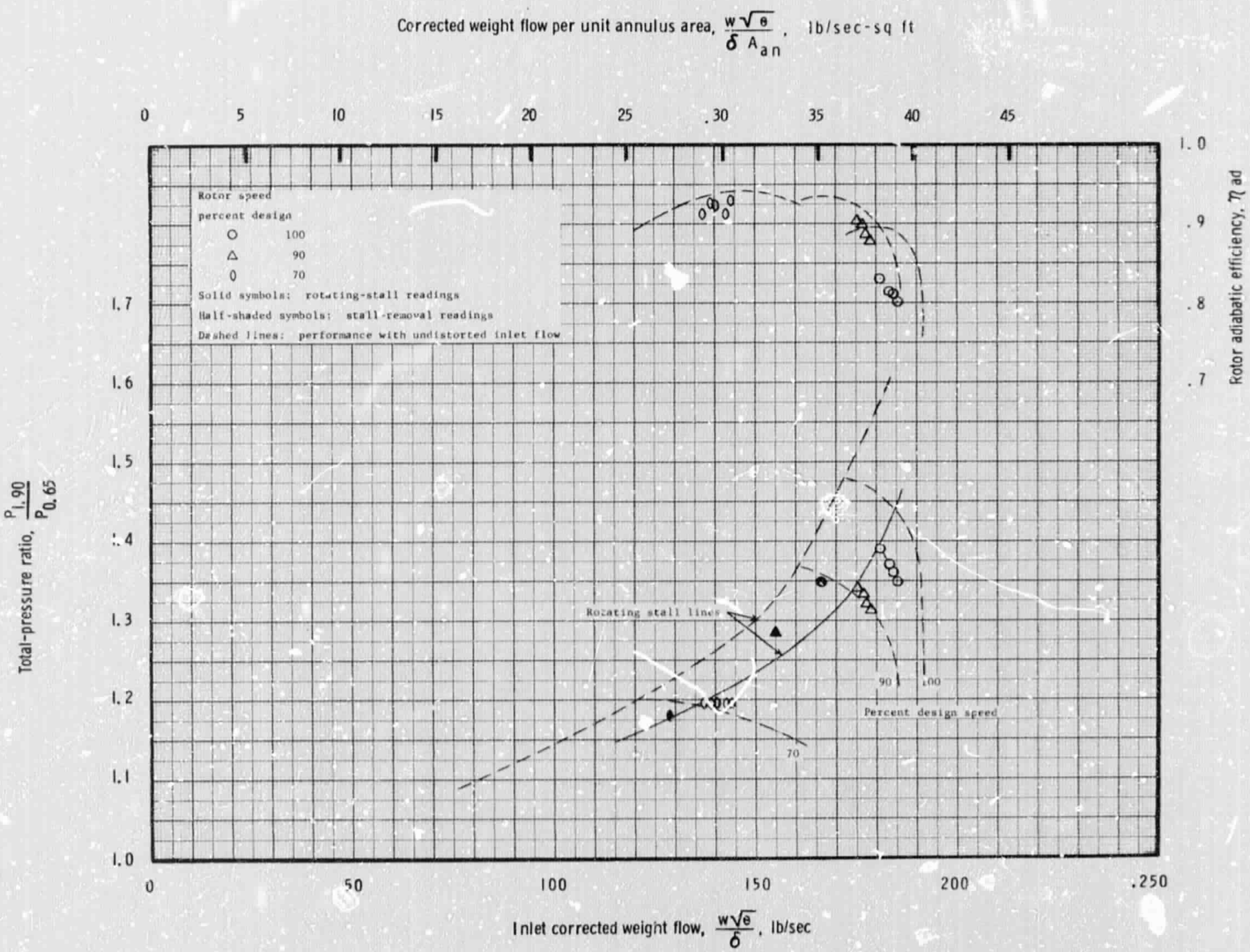


Figure 5 - Rotor performance map with radial inlet distortion

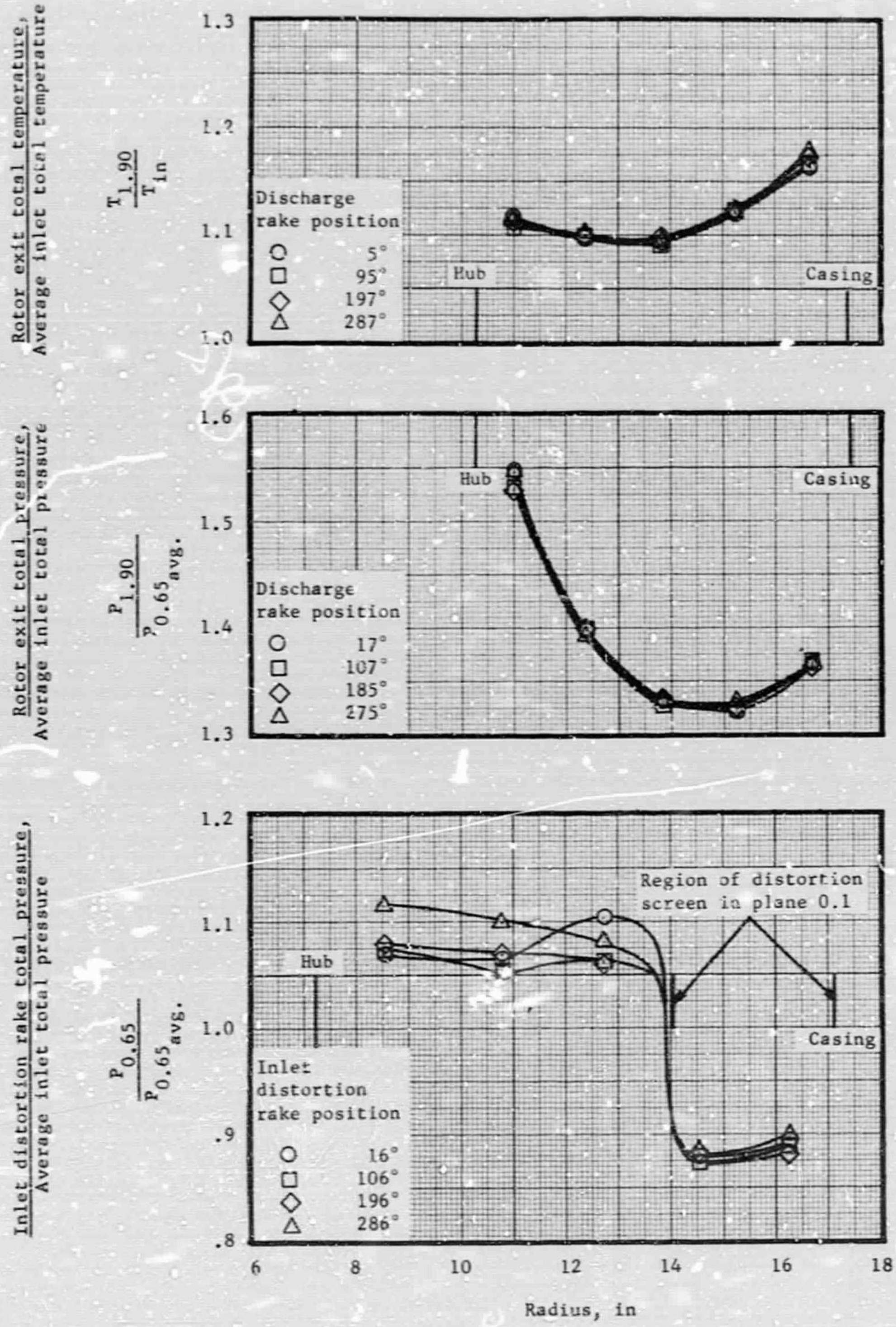


Figure 6. - Inlet total pressure, exit total pressure and exit total temperature profiles at 100% design speed, with radial inlet distortion, for Reading 45.

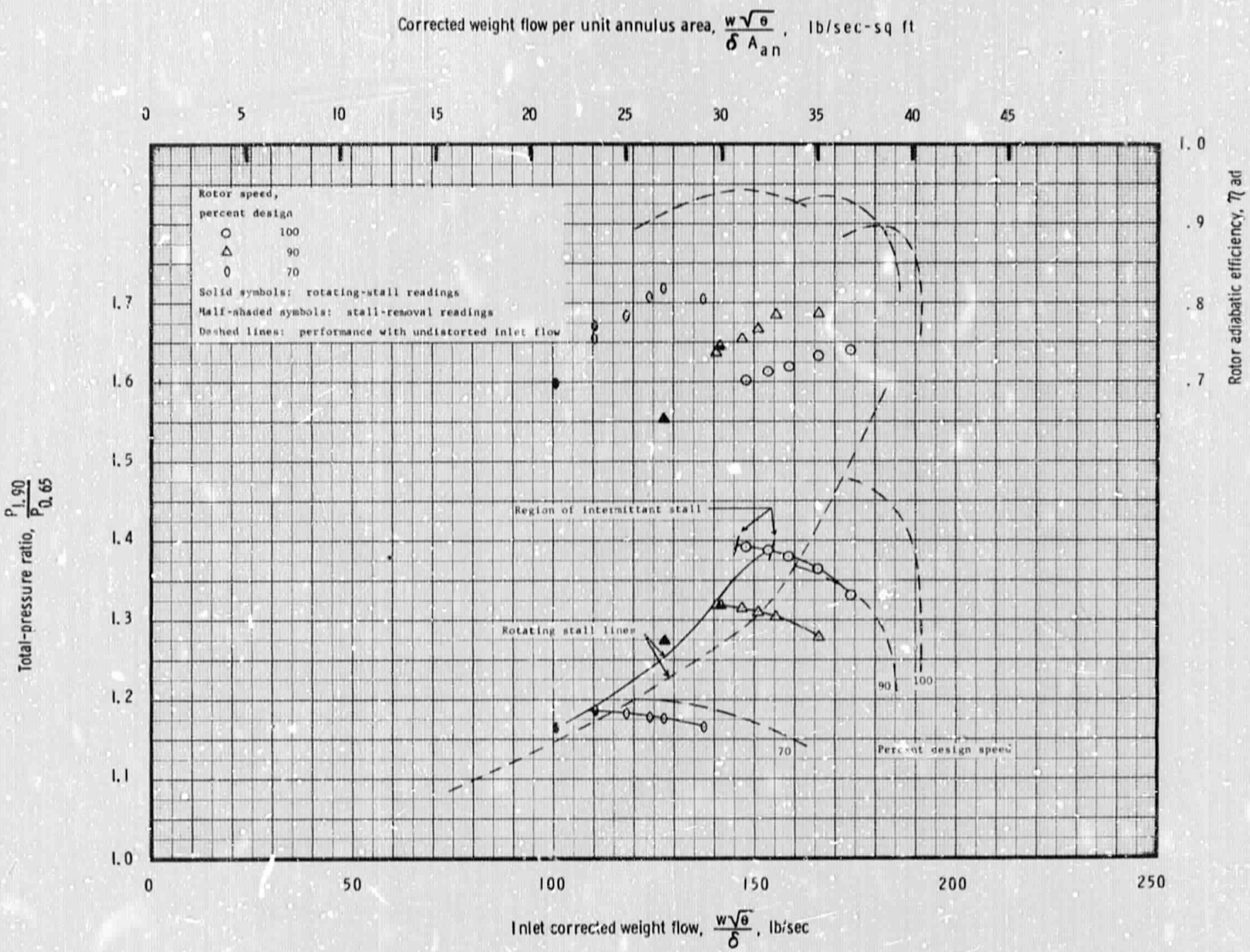


Figure 7 - Rotor performance map with heavy 90° circumferential inlet distortion

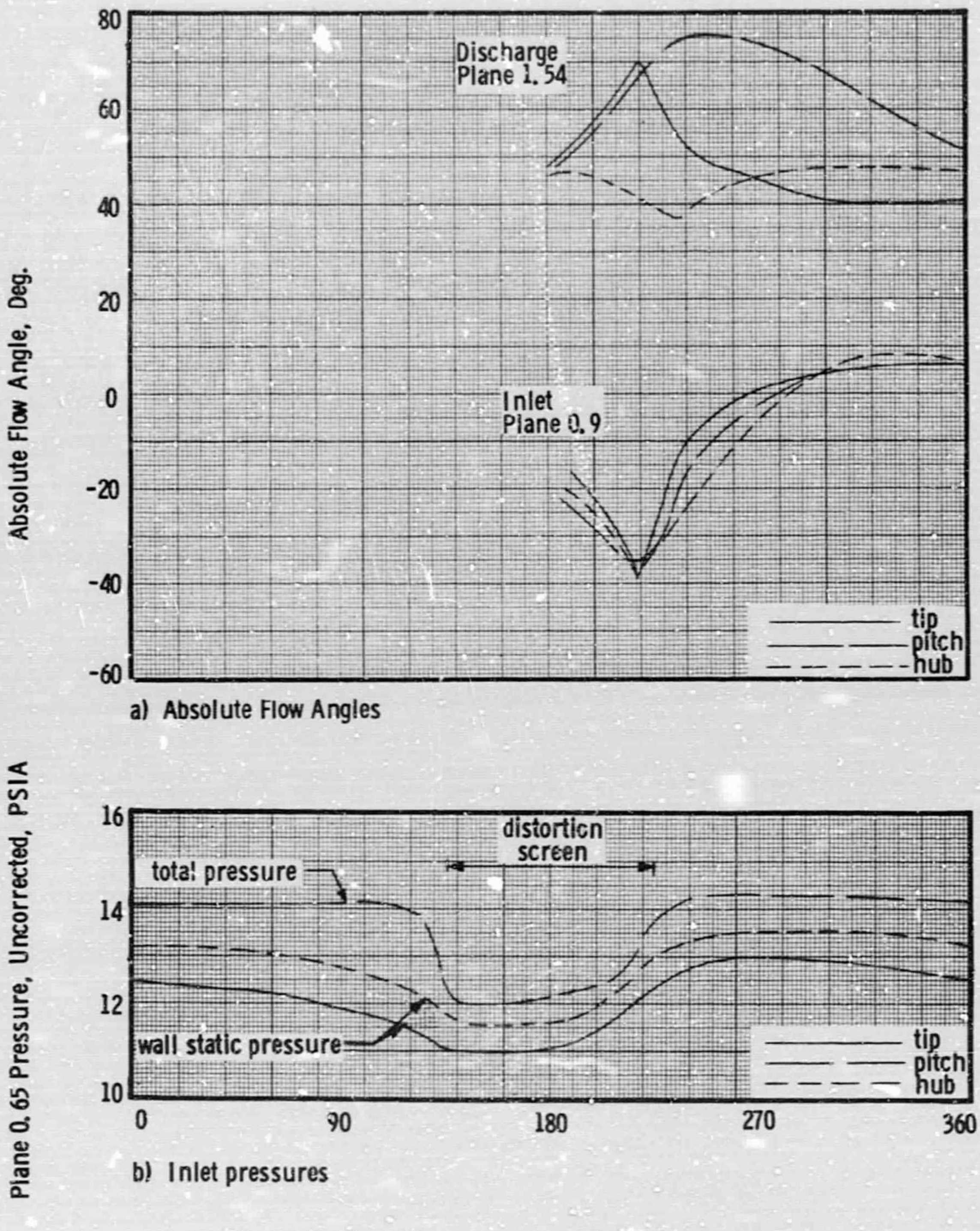


Figure 8 - Circumferential variation of fluid conditions with heavy 90° circumferential inlet distortion, for 100% design speed and discharge throttle valve setting equal to 10

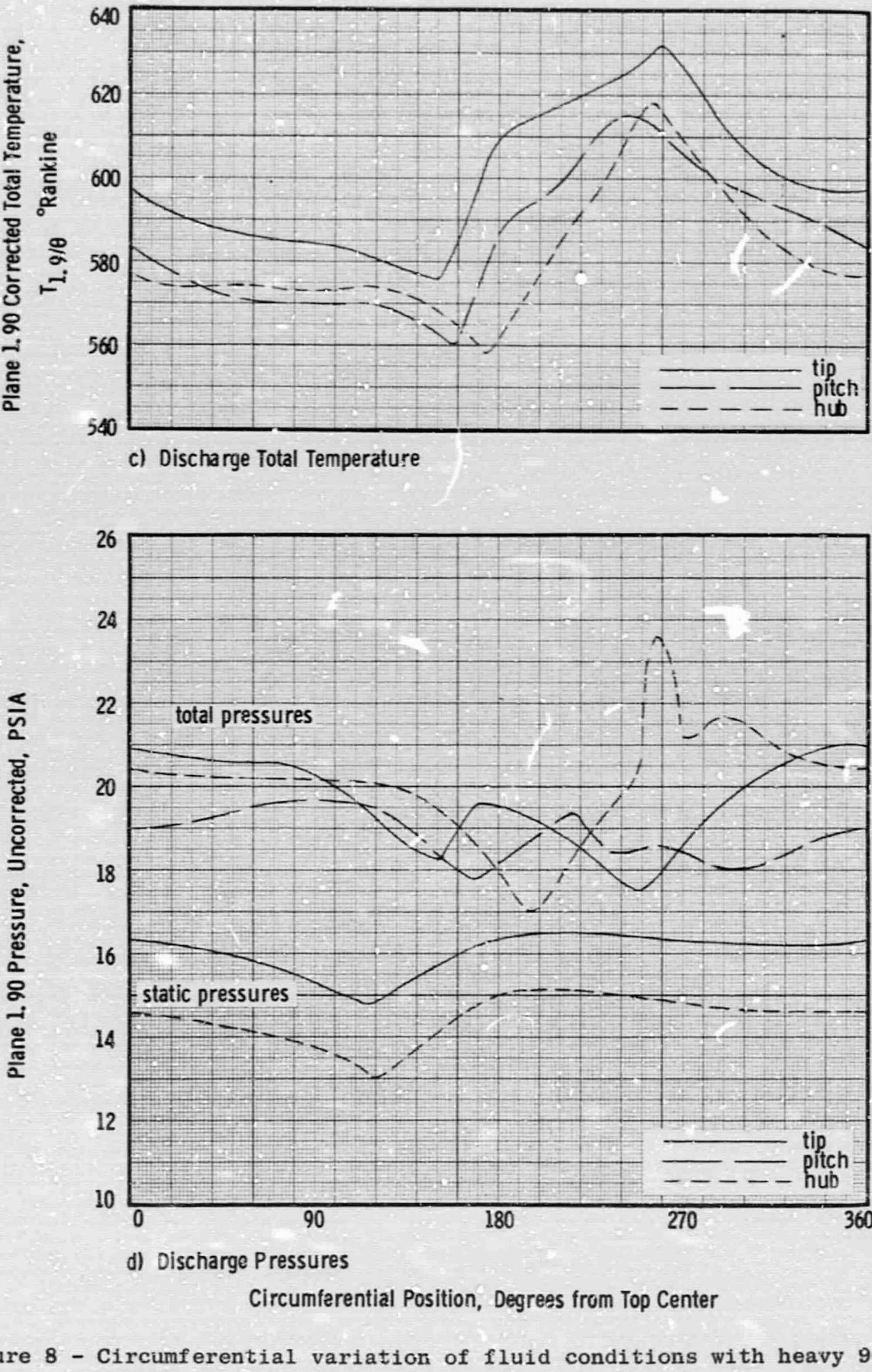


Figure 8 - Circumferential variation of fluid conditions with heavy 90° circumferential inlet distortion, for 100% design speed and discharge throttle valve setting equal to 10

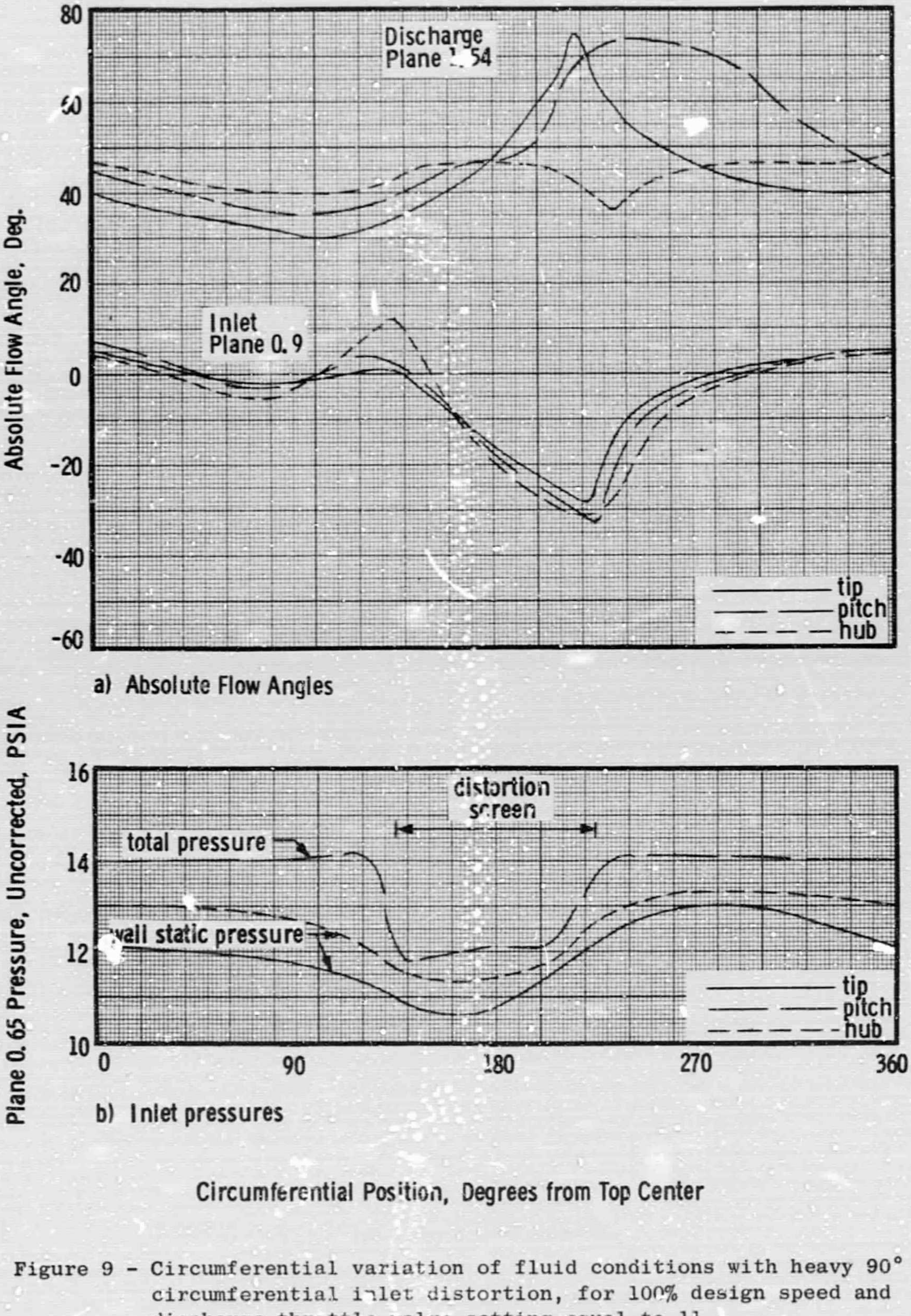


Figure 9 - Circumferential variation of fluid conditions with heavy 90° circumferential inlet distortion, for 100% design speed and discharge throttle valve setting equal to 11

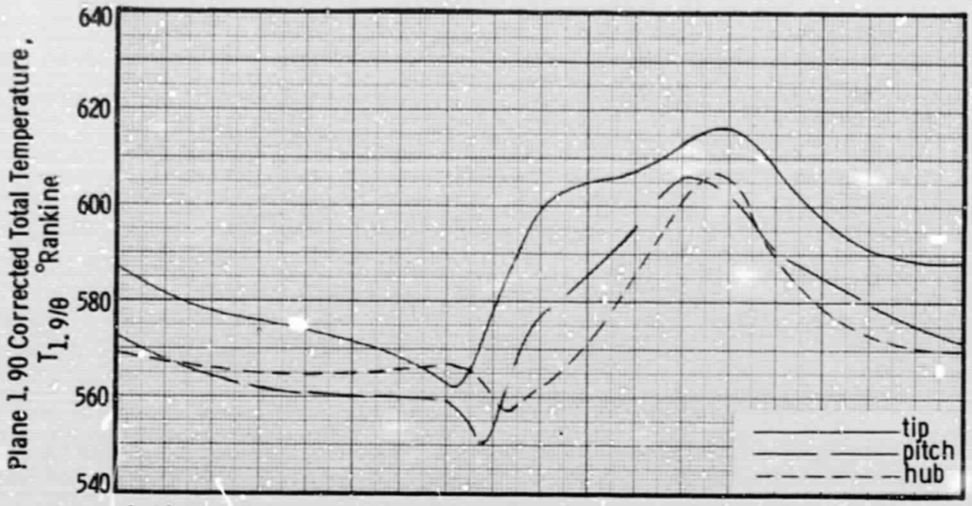


c) Discharge Total Temperature

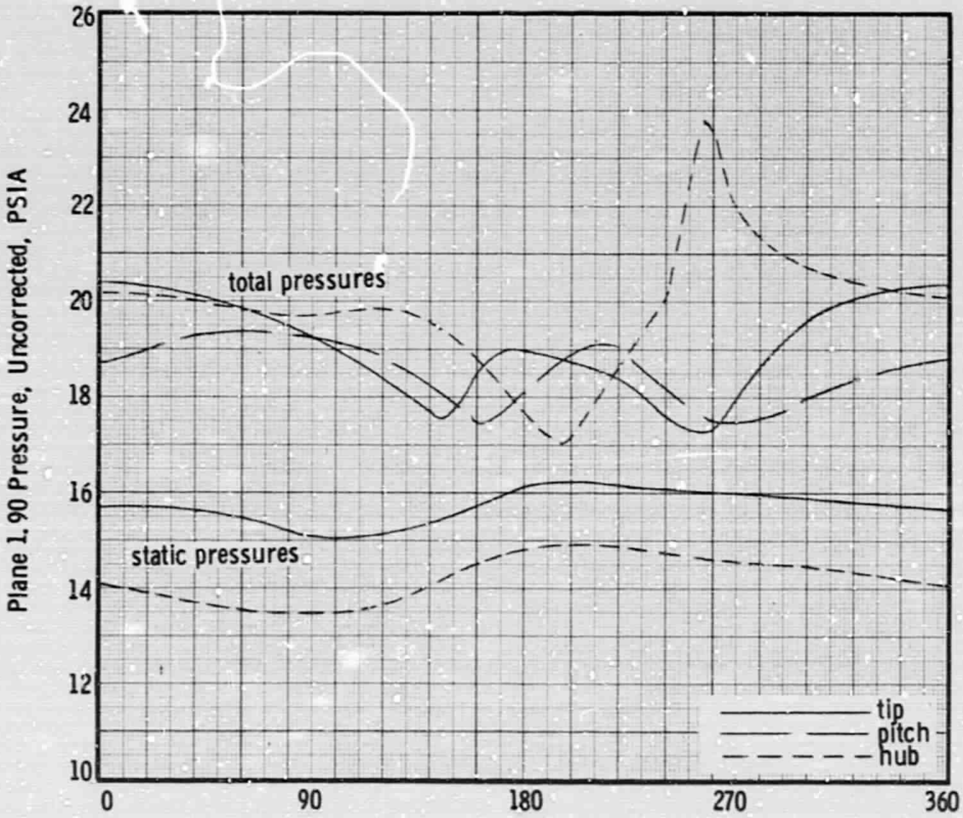


d) Discharge Pressures

Circumferential Position, Degrees from Top Center

Figure 9 - Circumferential variation of fluid conditions with heavy 90° circumferential inlet distortion, for 100% design speed and discharge throttle valve setting equal to 11

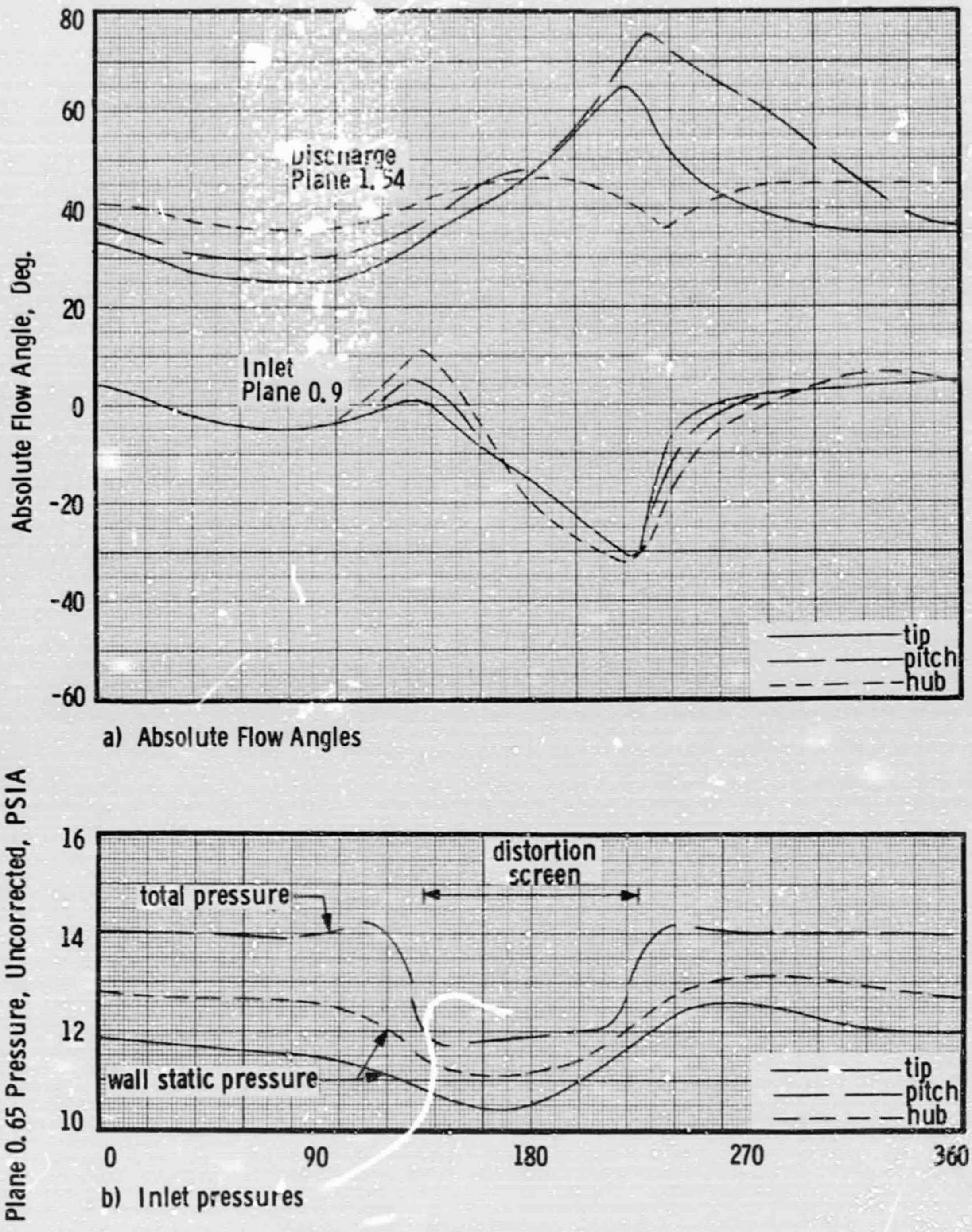


Figure 10 - Circumferential variation of fluid conditions with heavy 90° circumferential inlet distortion, for 100% design speed and discharge throttle valve setting equal to 18

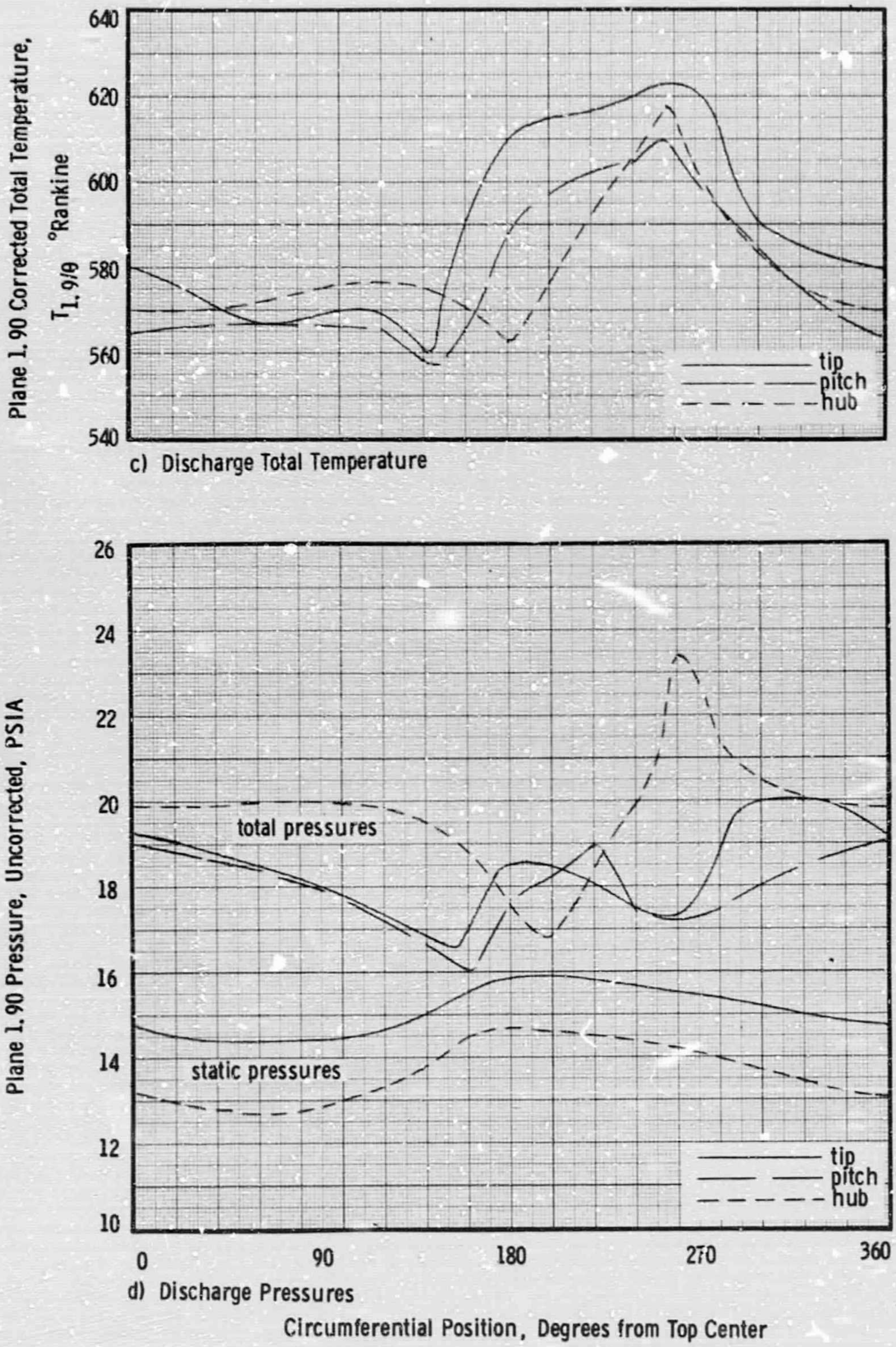


Figure 10 - Circumferential variation of fluid conditions with heavy 90° circumferential inlet distortion, for 100% design speed and discharge throttle valve setting equal to 18

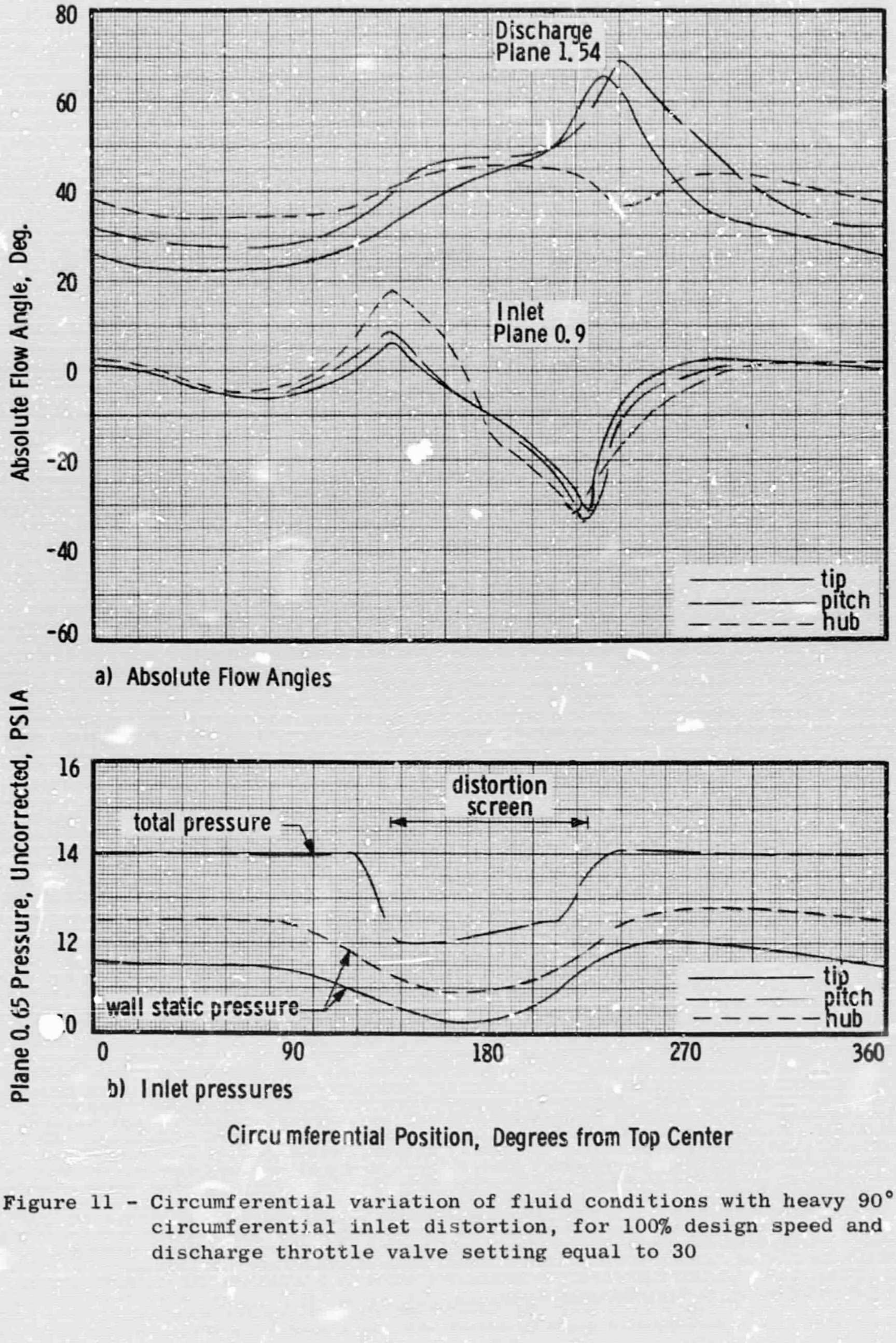


Figure 11 - Circumferential variation of fluid conditions with heavy 90° circumferential inlet distortion, for 100% design speed and discharge throttle valve setting equal to 30

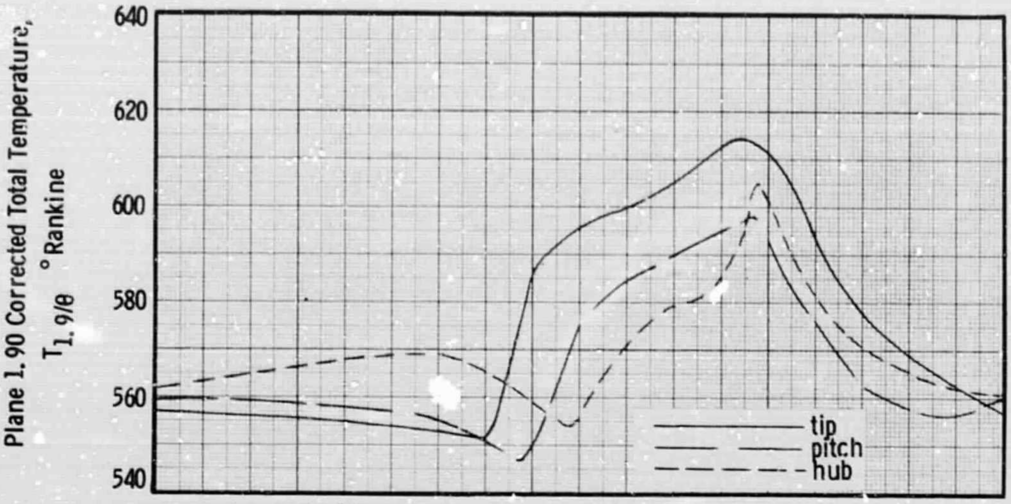


c) Discharge Total Temperature

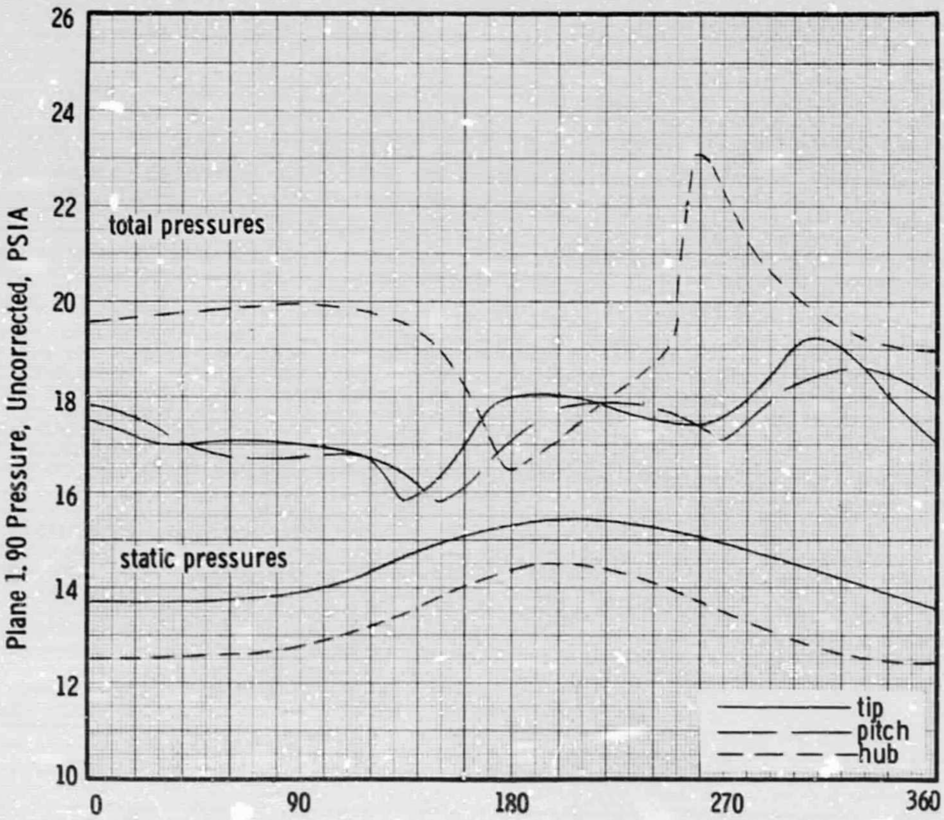


d) Discharge Pressures

Circumferential Position, Degrees from Top Center

Figure 11 - Circumferential variation of fluid conditions with heavy 90° circumferential inlet distortion, for 100% design speed and discharge throttle valve setting equal to 30

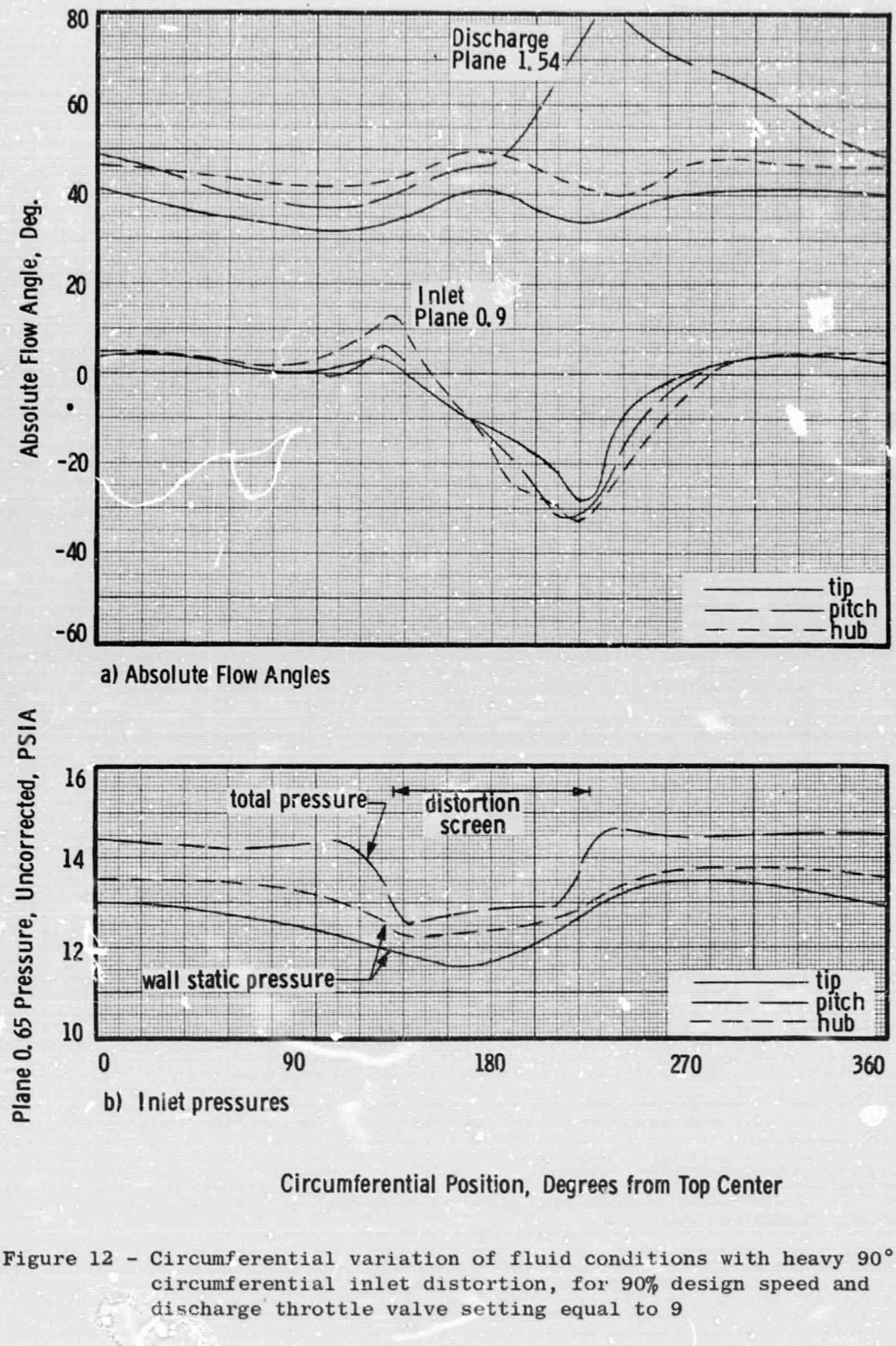


Figure 12 - Circumferential variation of fluid conditions with heavy 90° circumferential inlet distortion, for 90% design speed and discharge throttle valve setting equal to 9

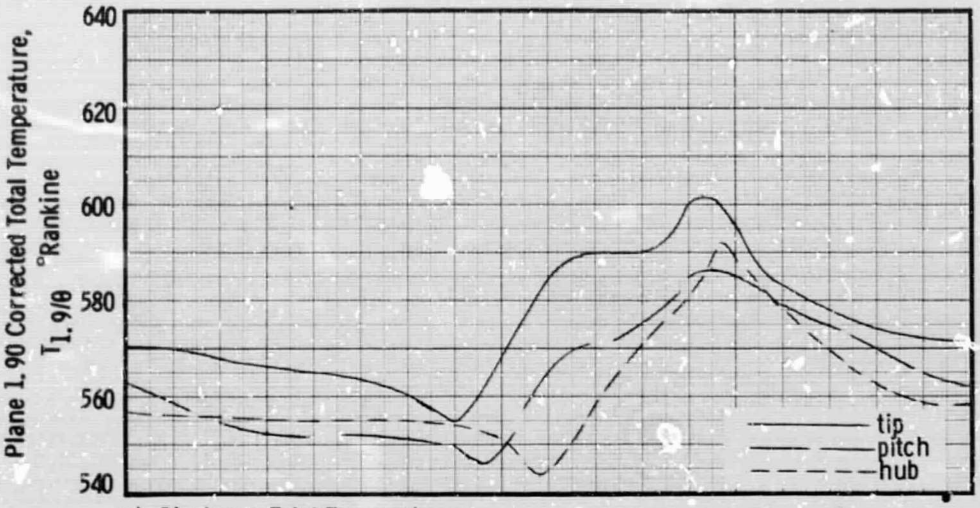


c) Discharge Total Temperature

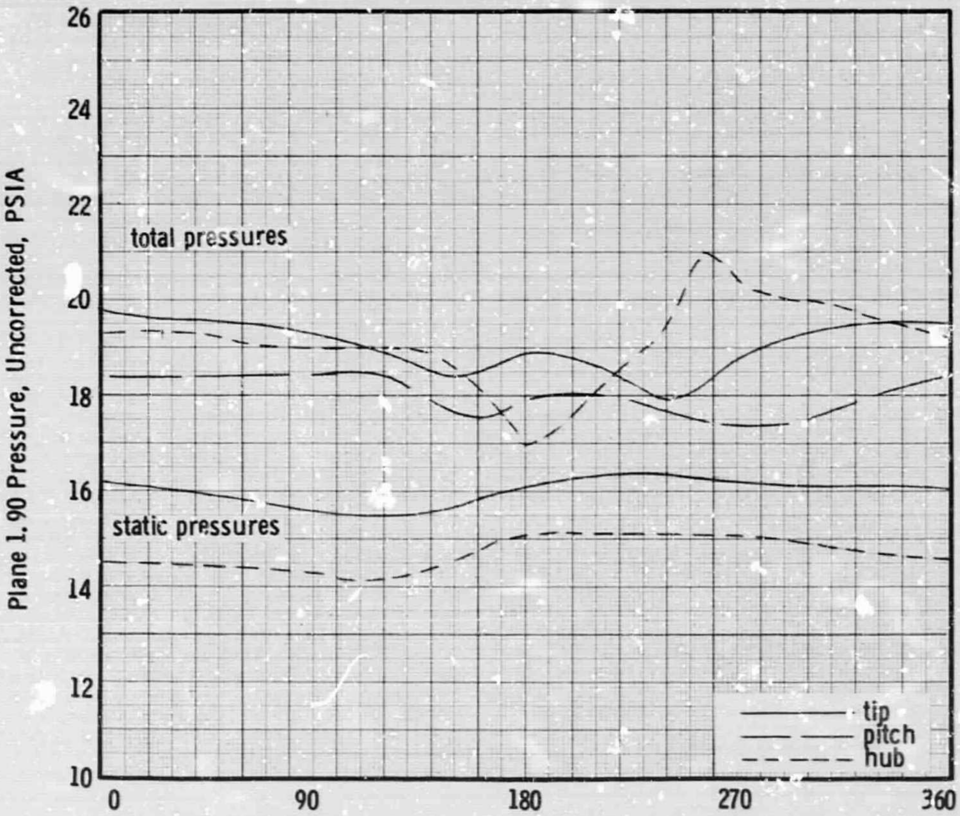


d) Discharge Pressures

Circumferential Position, Degrees from Top Center

Figure 12 - Circumferential variation of fluid conditions with heavy 90° circumferential inlet distortion, for 90% design speed and discharge throttle valve setting equal to 9

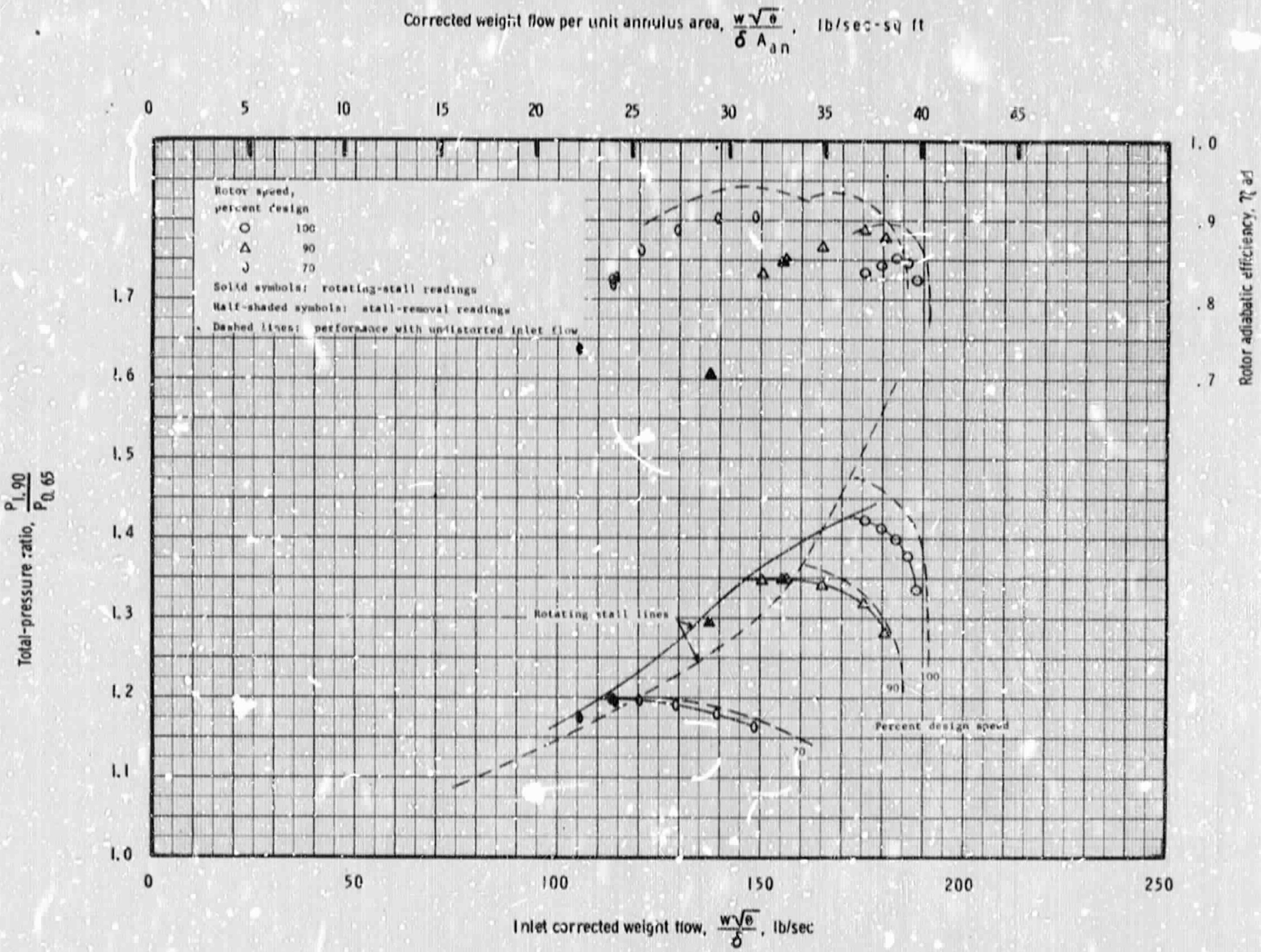


Figure 13 - Rotor performance map with light 90° circumferential inlet distortion

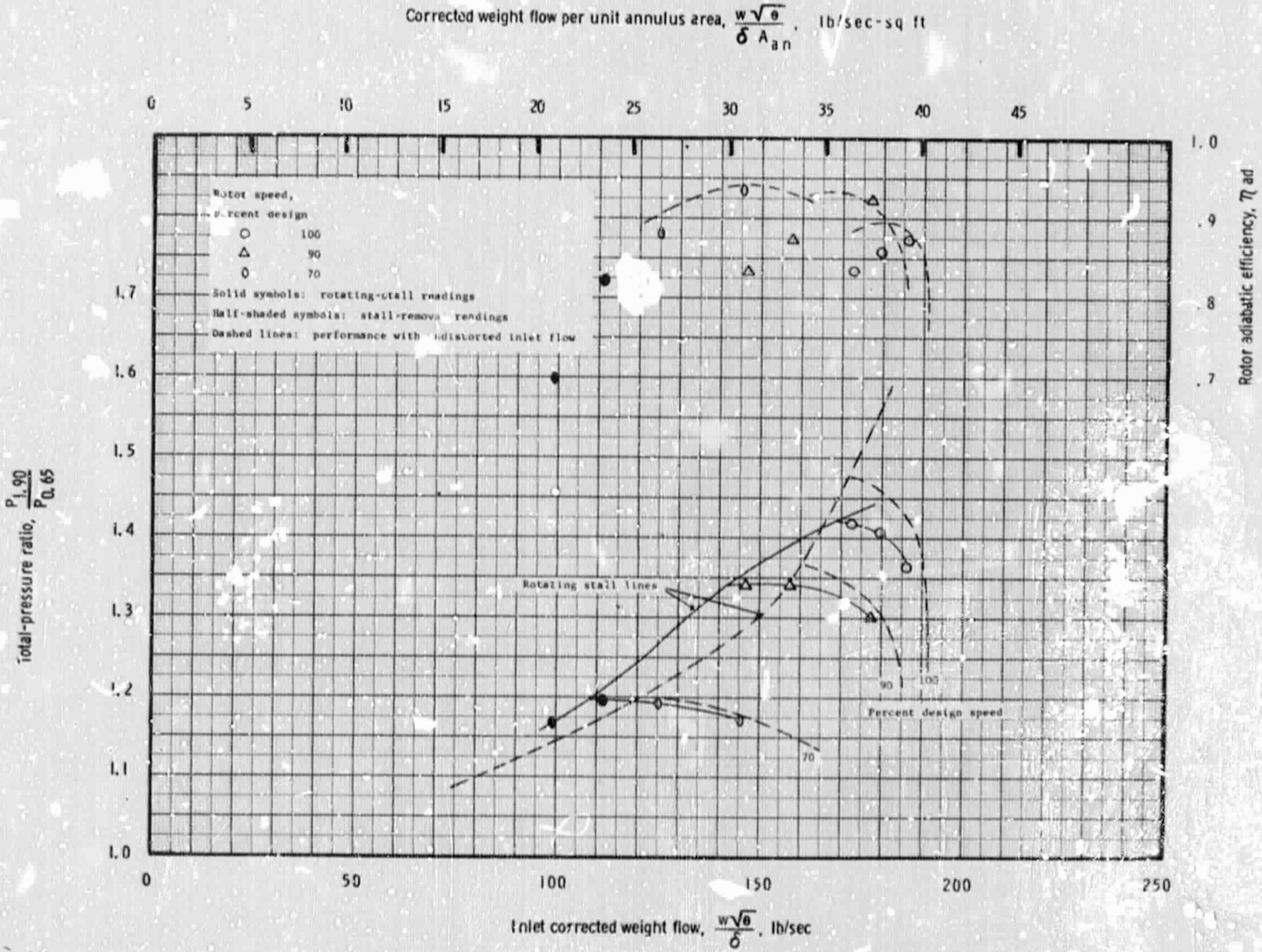


Figure 14 - Rotor performance map with light 180° circumferential inlet distortion

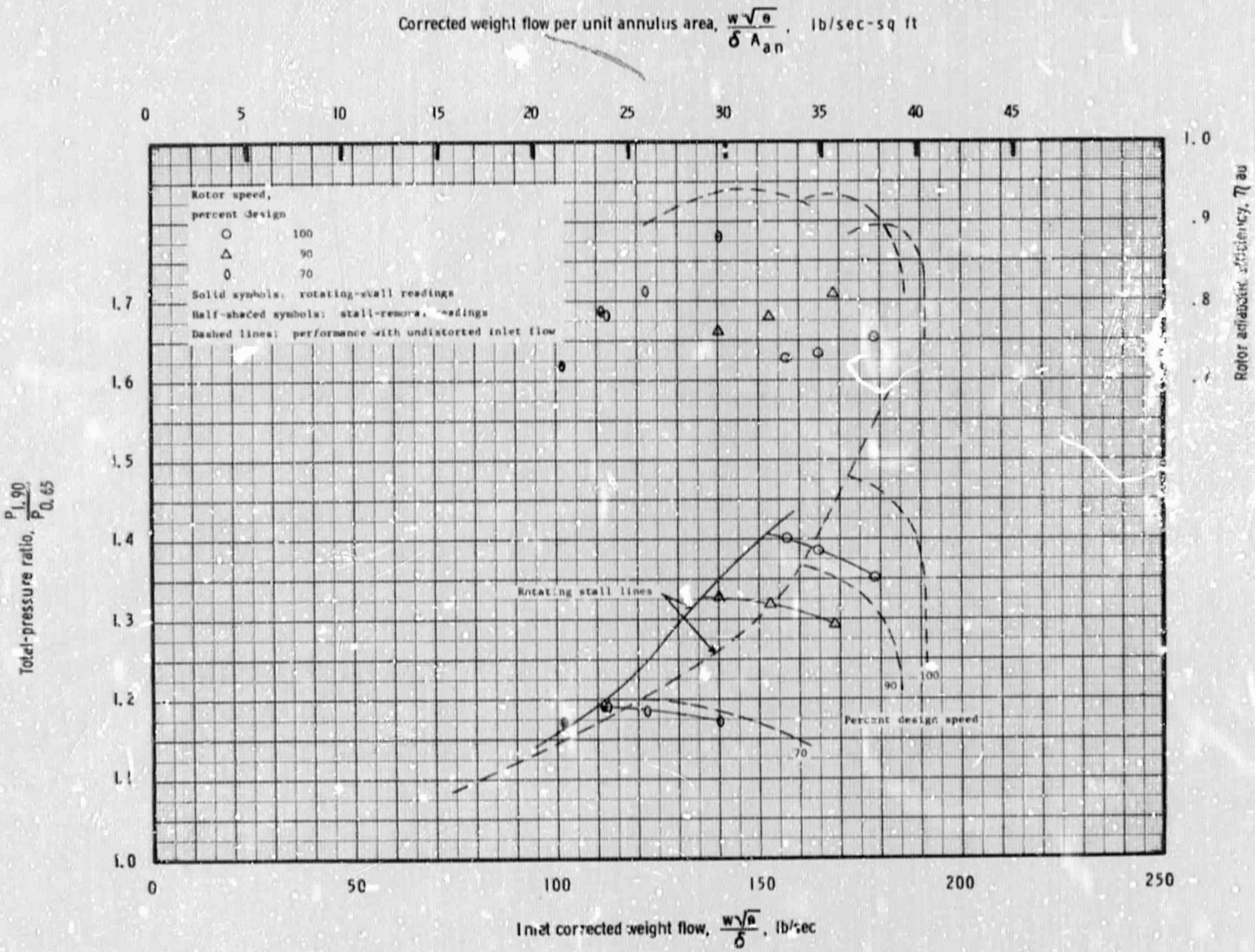


Figure 15 - Rotor performance map with rounded 120° circumferential inlet distortion

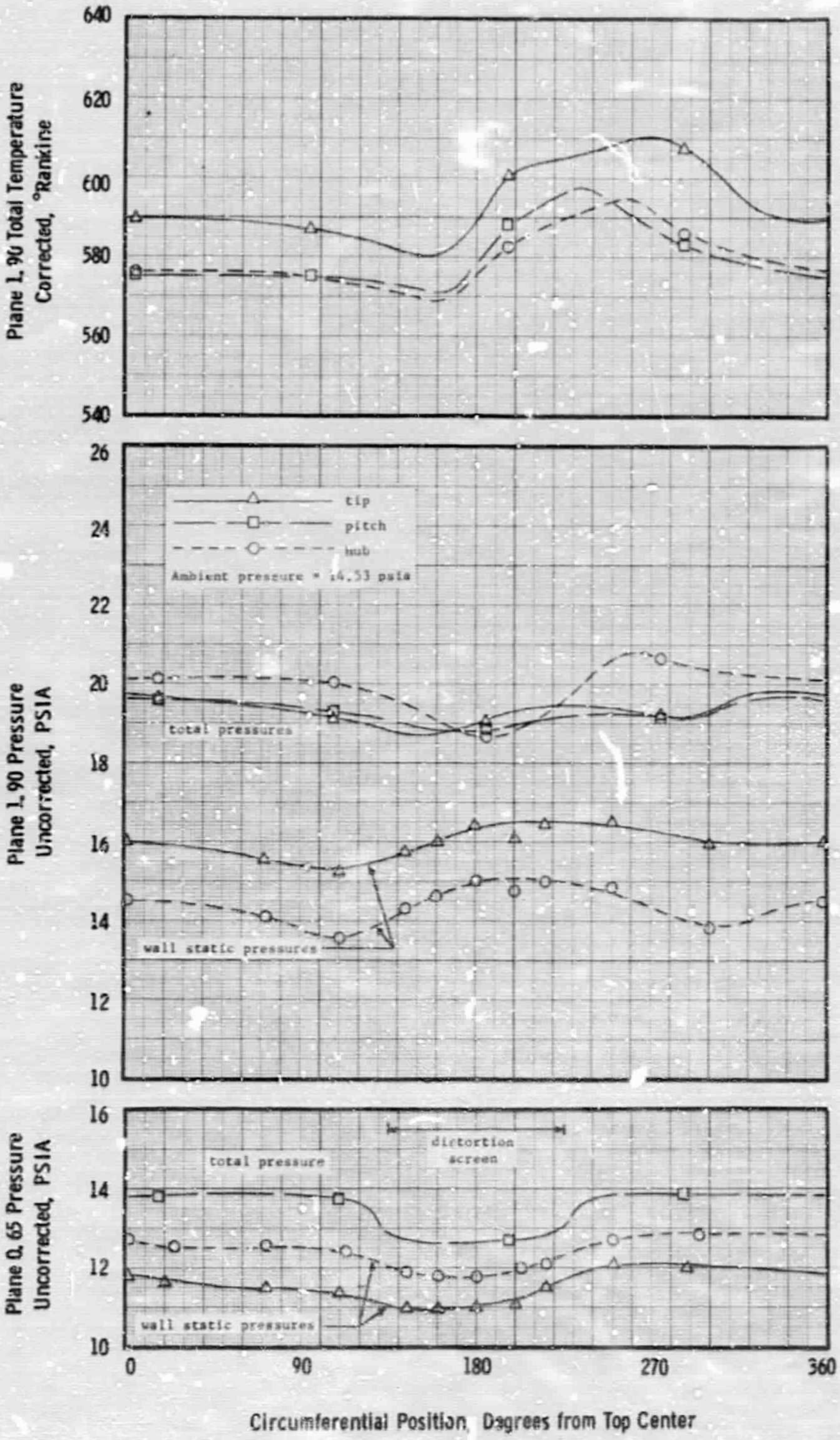


Figure 16. - Circumferential variation of fluid conditions with light 90° circumferential inlet distortion, at 100% design speed for Reading 57.

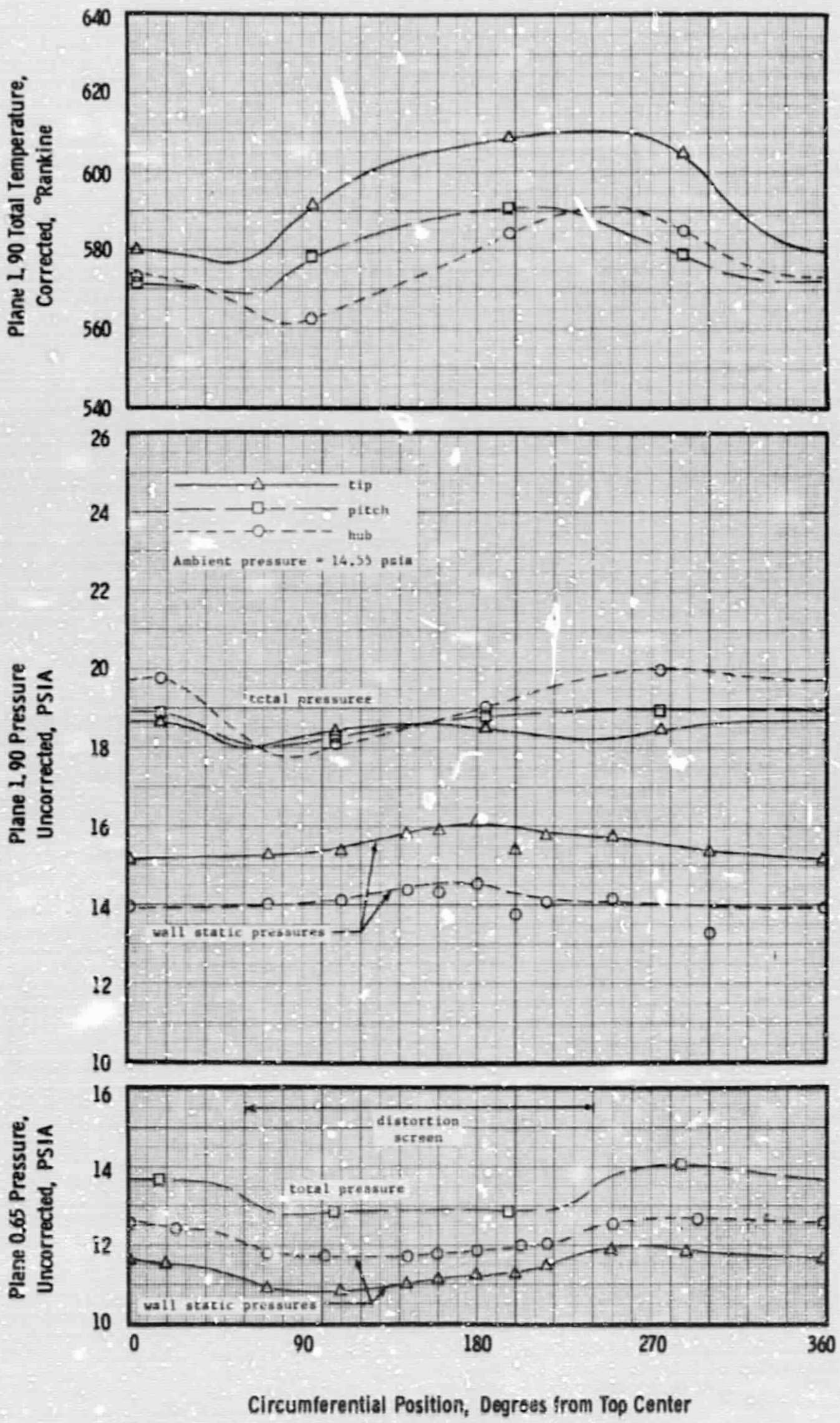


Figure 17. - Circumferential variation of fluid conditions with light 180° circumferential inlet distortion, at 100% design speed for Reading 77.

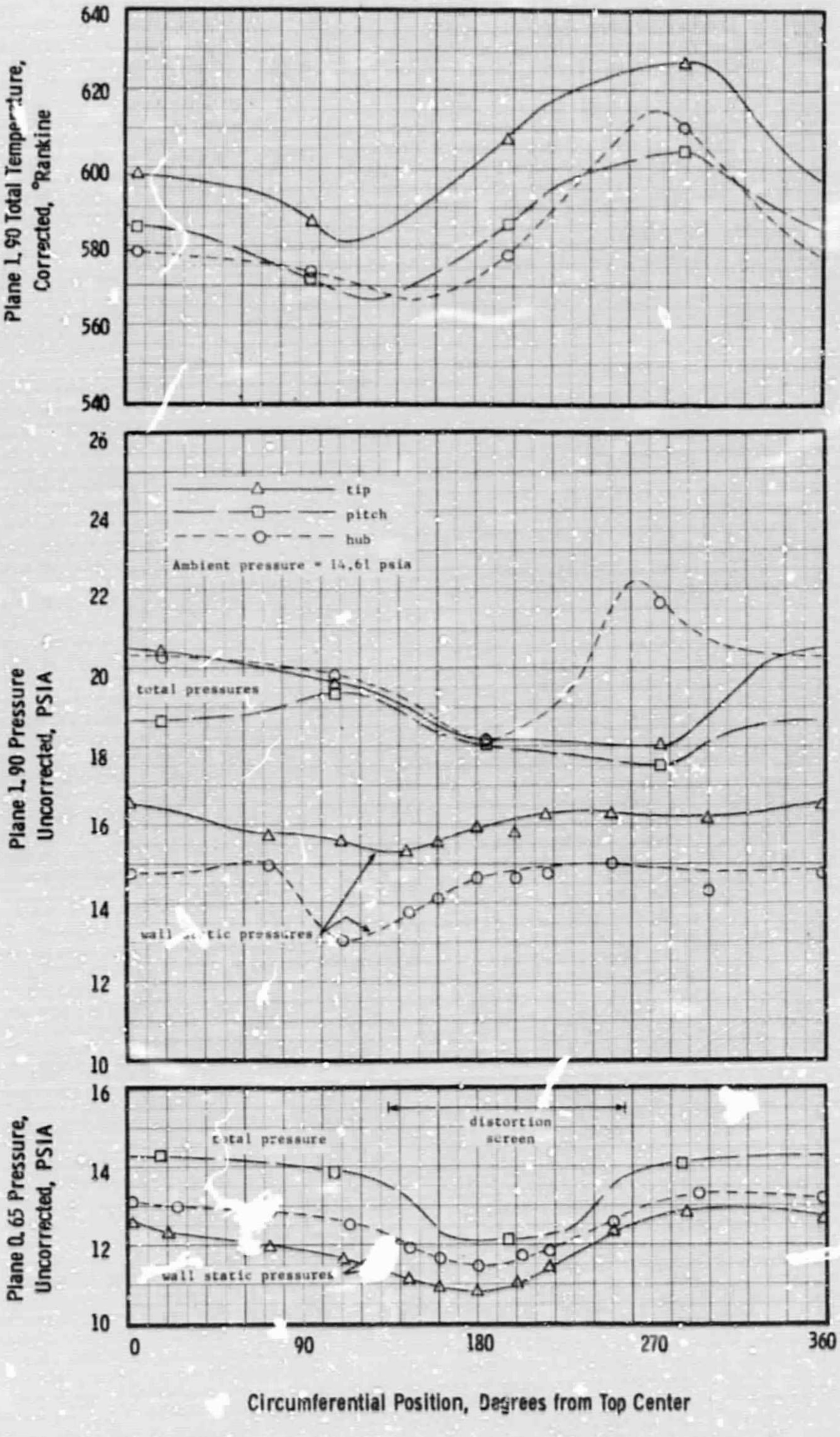


Figure 18. - Circumferential variation of fluid conditions with rounded 120° circumferential inlet distortion, at 100% design speed for Reading 86.